How turbidity currents dictate organic carbon fluxes across river-fed fjords

Sophie Hage[1,1], Valier Galy[2,2], Matthieu J.B. Cartigny[3,3], Catharina Heerema[4,4], Maarten S Heijnen[5,5], Sanem Acikalin[6,6], Michael Andrew Clare[5,5], Ian J W Giesbrecht[7,7], Darren Richard Gröcke[3,3], Alison Hendry[6,6], Robert George Hilton[4,4], Stephen M Hubbard[8,8], James Edward Hunt[9,9], Gwyn Lintern[10,10], Claire McGhee[11,11], Daniel R. Parsons[12,12], Ed L Pope[4,4], Cooper D Stacey[13,13], Esther Joanne Sumner[14,14], Suzanne Tank[15,15], and Peter Talling[16,16]

[1]Univ Brest, CNRS, Ifremer, Geo-Ocean
[2]woods hole oceanographic institution
[3]University of Durham
[4]Durham University
[5]National Oceanography Centre Southampton
[6]Newcastle University
[7]Hakai Institute and Simon Fraser University
[8]University of Calgary
[9]National Oceanography Centre, Southampton
[10]Geological Survey of Canada, Institute of Ocean Science
[11]University of Newcastle
[12]University of Hull
[13]Geological Survey of Canada
[14]University of Southampton
[15]University of Alberta
[16]University of Durham, U.K.

November 30, 2022

Abstract

The delivery and burial of terrestrial particulate organic carbon (OC) in marine sediments is important to quantify, because this OC is a food resource for benthic communities, and if buried it may lower the concentrations of atmospheric CO_2 over geologic timescales. Analysis of sediment cores has previously shown that fjords are hotspots for OC burial. Fjords can contain complex networks of submarine channels formed by seafloor sediment flows, called turbidity currents. However, the burial efficiency and distribution of OC by turbidity currents in river-fed fjords had not been investigated previously. Here, we determine OC distribution and burial efficiency across a turbidity current system within a fjord, in Bute Inlet (Canada). We show that 60 ± 10 % of the OC supplied by the two river sources, is buried across the fjord surficial (2 m) sediment. The sand-dominated submarine channel and its terminal lobe contain 63 ± 14 % of the annual terrestrial OC burial in the fjord. In contrast, the muddy overbank and distal flat basin settings contain the remaining 37 ± 14 %. OC in the channel, lobe and overbank exclusively comprises terrestrial OC sourced from rivers. When normalized by the fjord's surface area, at least three times more terrestrial OC is buried in Bute Inlet, compared to the muddy parts of other fjords previously studied. Although the long-term (>100 year) preservation of this OC is still to be fully understood, turbidity currents in fjords appear to be efficient in storing

OC supplied by rivers in their near-surface deposits.

How turbidity currents dictate organic carbon fluxes across river-fed fjords

S. Hage[1,2,3*], V.V. Galy[4], M.J.B. Cartigny[5], C. Heerema[6,5], M.S. Heijnen[7], S. Acikalin[8], M.A. Clare[7], I. Giesbrecht[9,10], D.R. Gröcke[11], A. Hendry[8], R. G. Hilton[12], S.M. Hubbard[2], J.E. Hunt[7], D.G. Lintern[13], C. McGhee[8], D.R. Pasons[14,] E. L. Pope[5], C D. Stacey[13], E.J. Sumner[3], S. Tank[15,9], P.J. Talling[5,11]

**Corresponding author: Sophie Hage (sophie.hage@ifremer.fr)*

[1]Univ Brest, CNRS, Ifremer, Geo-Ocean, F-29280 Plouzané, France

[2]Department of Geoscience, University of Calgary, Canada

[3]School of Ocean and Earth Sciences, University of Southampton, UK

[4]Department of Marine Chemistry and Geochemistry, Woods Hole Oceanographic Institution, MA USA

[5]Department of Geography, Durham University, UK

[6]Department of Geography, University of Victoria, Victoria, BC, Canada

[7]National Oceanography Centre Southampton, UK

[8]School of Natural and Environmental Sciences, Newcastle University, UK

[9]Hakai Institute, Vancouver, BC, Canada

[10]School of Resource and Environmental Management, Simon Fraser University, Burnaby, BC, Canada

[11]Department of Earth Sciences, Durham University, UK

[12]Department of Earth Sciences, University of Oxford, UK

[13]Geological Survey of Canada, Natural Resources Canada, Sidney, BC, Canada

[14]Energy and Environment Institute, University of Hull, UK

[15]Department of Biological Sciences, University of Alberta, Edmonton, Canada

- River-fed fjords incised by turbidity current systems can have a contemporary terrestrial organic carbon burial efficiency of 60 ± 10 %.
- Sandy surificial (2 m) deposits comprise 63 ± 14 % of the total terrestrial organic carbon burial budget in Bute Inlet, but only cover 17 % of the seafloor area.

- Global estimates based only on the muddy parts of fjords may significantly underestimate organic carbon burial rates by a factor > 3.

Abstract

The delivery and burial of terrestrial particulate organic carbon (OC) in marine sediments is important to quantify, because this OC is a food resource for benthic communities, and if buried it may lower the concentrations of atmospheric CO2 over geologic timescales. Analysis of sediment cores has previously shown that fjords are hotspots for OC burial. Fjords can contain complex networks of submarine channels formed by seafloor sediment flows, called turbidity currents. However, the burial efficiency and distribution of OC by turbidity currents in river-fed fjords had not been investigated previously. Here, we determine OC distribution and burial efficiency across a turbidity current system within a fjord, in Bute Inlet (Canada). We show that 60 ± 10 % of the OC supplied by the two river sources, is buried across the fjord surficial (2 m) sediment. The sand-dominated submarine channel and its terminal lobe contain 63 ± 14 % of the annual terrestrial OC burial in the fjord. In contrast, the muddy overbank and distal flat basin settings contain the remaining 37 ± 14 %. OC in the channel, lobe and overbank exclusively comprises terrestrial OC sourced from rivers. When normalized by the fjord's surface area, at least three times more terrestrial OC is buried in Bute Inlet, compared to the muddy parts of other fjords previously studied. Although the long-term (>100 year) preservation of this OC is still to be fully understood, turbidity currents in fjords appear to be efficient in storing OC supplied by rivers in their near-surface deposits.

Plain Language summary

Plants on land use CO2 in the atmosphere to produce organic carbon, which promotes their growth. Rivers transport organic carbon to the sea, where it is either eaten by fauna or buried in the seafloor, thus decreasing CO2 levels on Earth over thousands to millions of years. Fjords are recognized as global organic carbon sinks; trapping 18 million tons of organic carbon in their seafloor each year. However, the complex morphology of fjord seafloors was not considered in the calculation of this organic carbon flux. In this study we determine the distribution and abundance of organic carbon across a fjord (Bute Inlet, Canada), which contains a submarine channel network terminating onto a large accumulation of sand (called lobe). We show that

60 % of the organic carbon supplied by the two rivers connected to the fjord is buried across the fjord; the majority of this carbon being held in the channel and lobe. In total, Bute Inlet buries at least three times more organic carbon per surface area than other fjords previously studied. Submarine channels in fjords thus appear to promote the storage of land-derived organic carbon in the seafloor, potentially impacting CO2 levels and food resources for marine fauna.

1 Introduction

The sequestration of terrestrial particulate organic carbon (OC) in marine sediments can lead to a drawdown of atmospheric CO_2, and thus form a long-term control on carbon dioxide and oxygen levels in Earth's atmosphere (Berner, 1982, Burdige, 2007, Hilton and West, 2020). Terrestrial OC also constitutes a key energy resource for benthic communities living on the seabed, including in fjords (Hunter et al., 2013, Włodarska-Kowalczuk et al., 2019). It is therefore important to constrain the fluxes of terrestrial OC delivered to the seabed over short (decades to centuries) and long (thousand to million year) timescales. Major river deltas worldwide bury about 47 Mt of terrestrial OC each year, approximately 30 % of the total OC burial including marine organic matter in the oceans (Berner, 1989; Hedges & Keil, 1995; Burdige, 2007). Despite their surface areas being 40 times smaller than that of deltas and shelves, fjords have been shown to represent 17 % of the global terrestrial OC burial (Cui et al., 2016). Therefore, fjord systems are hotspots for OC sequestration (Smith et al., 2015, Cui et al., 2016, 2017). However, these global OC burial estimates in fjords are based on samples taken predominantly from the muddy parts of fjords, and assume the seafloor in fjords is homogeneous in terms of OC burial and sedimentation rates.

Fjord seafloors can, however, be highly heterogeneous (Smeaton and Austin, 2019; Bianchi et al., 2020) and comprise diverse sub-environments including submarine channels, and associated overbanks and lobes (Zeng et al., 1991, Conway et al., 2012, Pope et al., 2019). Such sub-environments are created by submarine sediment density flows, called turbidity currents. These flows distribute sediment and OC across the fjord floor, connecting river mouths to the deeper parts of fjords, and fractionate sediment and OC by grain size and density en-route. Only a handful of studies have discussed how OC is distributed and fractionated within fjords (Cui et al., 2016, 2017; Smeaton

and Austin, 2020; Bianchi et al., 2020; Hage et al., 2020). For example, a recent study of Scottish fjords revealed that muddy (<63 µm) sediments held the largest amounts of OC (~2.6 Mt) compared to sandy sediment (~0.26 Mt; Smeaton and Austin, 2020). While the OC budgets are known in the Scottish fjords, the processes determining these budgets remain uncertain, partly because of a lack of bathymetric data and knowledge of submarine flow processes in these settings (e.g. these Scottish fjords may not contain active turbidity currents). In contrast, a study of Bute Inlet (a fjord in British Columbia, Canada) highlighted that the sandy parts of a submarine channel formed by turbidity currents, held large amounts of OC, particularly compared to the overlying mud-rich sediments (Hage et al., 2020). However, the river-derived OC inputs and burial rates in different sub-environments created by turbidity currents were not considered in that previous study of Bute Inlet, nor in any other fjord. Given the large variation and uncertainty in OC burial efficiency between fjord sub-environments, it is important to assess this variability more accurately to estimate global OC budgets (Burdige, 2007, Smith et al., 2015) and to improve paleoclimate/environmental reconstructions based on sediment cores in fjords (Bianchi et al., 2020).

Here for the first time, we quantify the amount and type of OC supplied by two rivers and its distribution in the surficial sediments (top two meters) of different turbidity current sub-environments (e.g. channel floor, overbanks, lobe, distal basin) across a river-fed fjord. This study then shows how OC is unevenly distributed within a fjord, and illustrates how OC distribution and burial is dependent on turbidity current processes. Insights into how OC is distributed have wider implications for understanding OC burial by turbidity currents in locations other than fjords, for which there are also very few detailed OC budgets from river sources to marine sinks. Therefore, we compare our Bute Inlet results with available information on how OC is distributed in sandier or muddier sub-environments of other turbidity current systems, i.e. Gaoping (Kao et al., 2014, Liu et al., 2016), Ganges-Brahmaputra (Galy et al., 2007, Lee et al., 2019), Congo (Baudin et al, 2020). This comparison highlights whether similar or contrasting OC burial patterns emerge more generally.

The main objective of this paper is to constrain OC fluxes from source-to-sink in Bute Inlet by answering the following questions: 1) How much OC

is delivered by the two rivers discharging into Bute Inlet? 2) How much and what type of OC is present in the Bute Inlet sub-environments? 3) What is the terrestrial OC burial efficiency of Bute Inlet and how does it compare with other fjords? Finally, we discuss the study in a wider global context, and thus compare our results from Bute Inlet with (non-fjord) deep-sea turbidity current systems.

2 Bute Inlet: a fjord fed by two rivers

Bute Inlet is a 78 km-long fjord in British Columbia, Canada (Fig. 1). The inlet has an average width of ~4 km, an average depth of 550 m (with a maximum of 660 m; Prior et al., 1987), and a total surface area of 273 km^2 (including the fjord's steep sidewalls).

2.1 Homathko and Southgate Rivers

The Homathko and Southgate Rivers feed the head of Bute Inlet (Fig. 1). Both rivers are supplied by meltwater from snow and glaciers within their catchment and by moderate to high levels of precipitation from a rainforest climate in the coastal mountain catchments (1684 and 2089 mm of mean annual precipitation were recorded between 1981 and 2010 in the Homathko and Southgate Rivers, respectively; Giesbrecht et al., in press). The river floodplains are populated by coniferous and deciduous forests. These two rivers provide 94 % of the freshwater and sediment inputs into the fjord, with the remainder of the freshwater being provided by small streams entering the fjord at its margins (Farrow et al., 1983). The watershed areas are 5782 km^2 and 1985 km^2 for Homathko and Southgate Rivers, respectively (Fig. 1; Gonzalez et al., 2018). The Homathko River has an average annual discharge of 250 m^3/s, with an average summer peak discharge of ~800 m^3/s, in response to melting snow and ice (Water Survey of Canada, 2020). The average annual suspended sediment load of the Homathko River is 30 kg/s, whereas its bedload is 99 kg/s (Table 1; Syvistki and Farrow, 1983). There was no gauging station in the Southgate River up to 2021. However, recent (2021) data and the co-variation between daily discharge on the two systems allowed the Southgate discharge (water and total suspended load) to be modelled for our years of interest (Table 1; Texts S1 to S4).

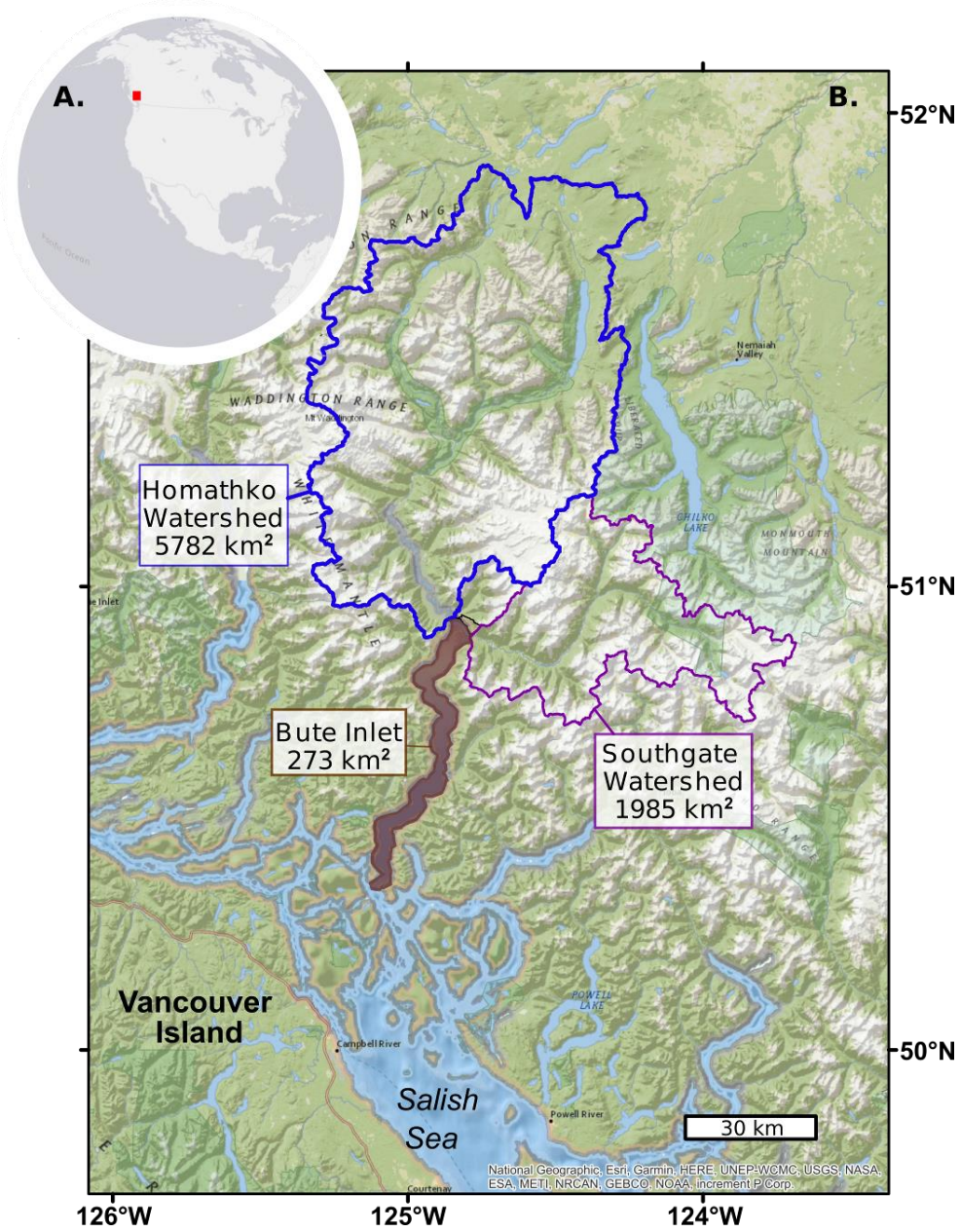

Figure 1: *A. Location of Bute Inlet in British Columbia (Canada). B. Bute Inlet is fed by Homathko and Southgate Rivers. Watershed areas were delimited by Gonzalez et al. (2018)*

During the spring thaw (freshet), the rivers create large sediment-laden freshwater plumes at the fjord's head (Tabata and Pickard, 1957, Syvitski et al., 1985). These plumes flow on top of the more saline fjord water, thereby bringing terrestrial particles into the fjord and enhancing the heterotrophic activity of bacterioplankton (Albright, 1983). Due to the relatively large tidal range (up to 5.5 m), sediment from these river plumes

is likely to be concentrated in a turbidity maximum that is located in between the fresh and saline water (Dyer, 1997). Observations in a similar and nearby fjord setting (Howe Sound, Canada), show that during the freshet these turbidity maxima can hold enough sediment to become denser than the saline fjord water (Hage et al., 2019). During spring tide, the river plume becomes more focused and powerful, so that low tides cause these dense turbidity maxima to migrate onto the steep delta-slope, where they can trigger turbidity currents (Hage et al., 2019). These processes, together with submarine failures of the delta slopes, result in turbidity currents frequently being triggered in such river-fed and tide-influenced fjord settings (Clare et al., 2016; Hizzett et al., 2018). It is likely that similar initiating mechanisms for turbidity currents also occur in Bute Inlet (Hughes Clarke et al., 2015).

	Homathko	**Southgate**
Watershed Area (km^2)	5782	1985
Contribution to Bute Inlet (%)[a]	75	19
Yearly mean discharge (m^3/s) [a]	254	141
Yearly mean suspended load (Kt/yr) [b]	946	221
Yearly mean bedload (Kt/yr)	4164[b,c]	
Average TOC in river suspended load (%)	0.35 ± 0.1	
Average TOC in river bedload (%)	0.15 ± 0.07	0.56 ± 0.1
OC flux in river suspended load (Kt OC/yr)	8.4 ± 1.6	
OC flux in river bedload (Kt OC/yr)	14.9 ± 3.6	
Total riverine OC flux (Kt OC/yr)	**23.4 ± 5.2**	

Table 1*: Homathko and Southgate Rivers characteristics and estimates of annual organic carbon fluxes. a: Syvtiski and Farrow (1983). b: see Text S1 for suspended load estimates in both rivers. c: no bedload estimate was found in the literature for the Southgate River. The bedload was thus estimated based on the Homathko River using the ratio between the two river watersheds as a scaling factor (Text S2).*

2.2 Bute Inlet turbidity current system

Downstream of the Homathko and Southgate Deltas lie two submarine channels, which merge into a single sinuous channel formed by turbidity currents (Prior et al., 1986, 1987; Fig. 3). The channel is incised into the seafloor to a depth of up to 55 m. The channel floor is flanked by terraces that are particularly well-developed in the first 10 km of the fjord. Further downstream (430-580 m water depth) the submarine channel becomes less incised and is flanked by levees that are variably developed (Prior et al. 1987). For simplicity, in this paper we use the term "overbanks" to describe both the muddy terraces and levees bounding the submarine channel floor in Bute Inlet along its entire length.

The sediment composition of the Bute Inlet turbidity current system has been described in older work, based on sediment cores (Prior et al., 1986, Zeng et al., 1991), yet the OC composition of these cores was not documented until recently. The OC stored within the submarine channel floor was shown to be composed mostly of young terrestrial woody debris buried within fine sands (Hage et al., 2020). In this study, we build on the findings of Hage et al. (2020) from the channel floor, by documenting the distribution of OC across all of the sub-environments within this turbidity current system (i.e. channel floor, overbanks, lobe and distal flat basin). We also build on previous work on repeated bathymetric surveys and core dating (Heijnen et al., in review; Syvitski et al., 1988) to derive sedimentation rates and OC burial fluxes across the fjord.

3 Materials and Methods

3.1 River sampling

We used 22 samples to characterize OC supply from the rivers. These samples cover a range of grain size classes as they were collected within the river waters, on the river banks, delta-top plains, and in the river plumes at the fjord surface (Fig. 2). The sampling campaign was conducted on 26 October 2017 (Figs. 2 and 3; Fig. S3), when the Homathko River discharge was 390 m^3/sec (Water Survey of Canada, 2020). This is higher than the 250 m^3/sec average annual river discharge on the Homathko River, and lower

than its ~800 m^3/sec average summer peak discharges (Water Survey of Canada, 2020).

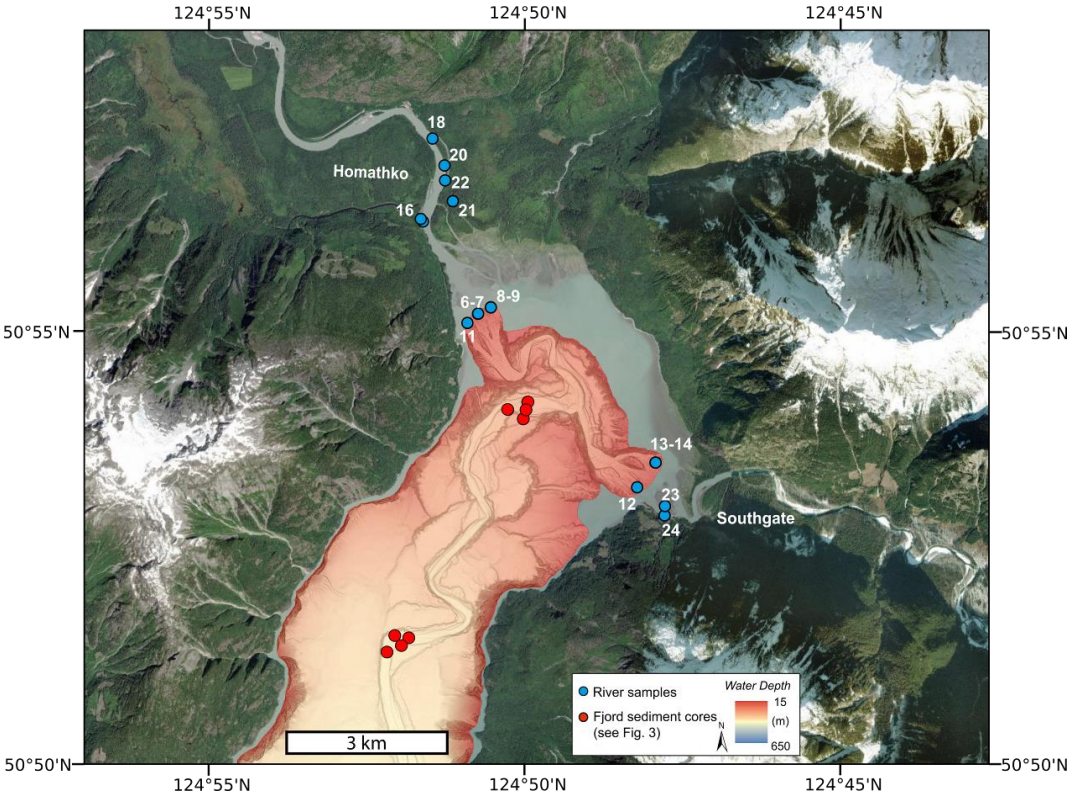

Figure 2: *Bathymetry of the head of Bute Inlet (collected in 2008 by the CCGS Vector), also showing locations of sediment samples collected in Homathko and Southgate Rivers in 2017, and offshore in fjord sediments in 2016.*

3.2 Fjord sampling and definition of sub-environments

Two field campaigns were conducted in June 2016 and October 2016 to sample the fjord sediments. In total, we use a set of 15 sediment cores, which sampled the upper 30 to 200 cm of recent seabed sediment. These cores were located across all sub-environments of the fjord's seabed, including the sandy channel floor and lobe, as well as the muddy overbank and distal flat basin (Fig. 3). We have few constraints on the characteristics/extent of turbidity current overbank flows, so we infer the overbank's external limit as the base of the fjord walls (red outlined area in Fig. 3). We note that sediment cores from these overbank areas are located relatively close to the sandy channel. A sediment core at the end of the fjord (650 m water depth) is used to characterize the OC composition for the entire distal flat basin (core 15;

light blue outlined area in Fig. 3). We have no samples on the steep fjord sidewalls; hence these areas are not included in our OC analyses.

Visual logging identified sandy and muddy facies within the sediment cores (Fig. 3e, f). A total of 99 sub-samples were collected from the fjord sediment cores, to ensure representative sampling of each of the facies that were present in the channel floor, overbanks, lobe and distal flat basin. All samples were analyzed for carbon geochemistry, as described below.

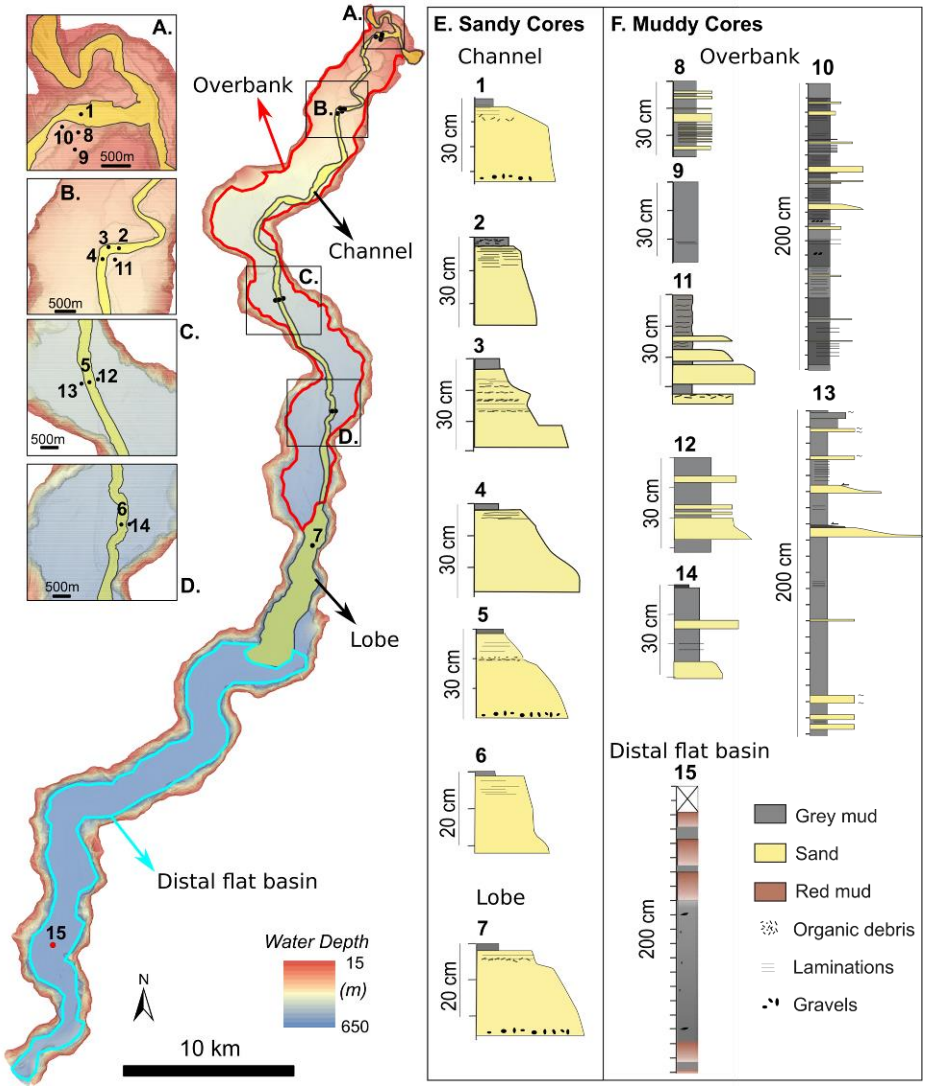

***Figure 3**: Submarine morphology and sediment cores collected in the Bute turbidity current system. Boxes A to D: zoom-ins showing the parts of the system bounded by overbank. E & F: Sediment core set. 30 cm long cores were collected using a box coring system; 200 cm long cores were collected using a piston coring system.*

3.3 Geochemistry on river and fjord samples

Total carbon was measured on all river and fjord samples using an LECO elemental analyzer. All samples were also analyzed for total organic carbon (TOC) content after trace amount of inorganic carbon (carbonate) were removed using HCl and rinsing with milli-Q water. No effervescence was observed during this acidification step, confirming minimal carbonates in the system (Fig. 4). TOC measurements allowed for quantifying the total amount of OC delivered by the rivers and buried in the different fjord sub-environments. In order to constrain the type (terrestrial or marine) of OC, all samples were analyzed for carbon stable isotopes ($\delta^{13}C$) using an isotope ratio mass spectrometer. Terrestrial organic matter derived from C3 plants has an average $\delta^{13}C$ between -26 and -28 ‰ (Hecky and Hesslein, 1995) and can reach values as low as -31 ‰, which correspond to young woody debris (Hage et al., 2020). In contrast, marine organic matter preserved in northeast Pacific sediments has an average $\delta^{13}C$ of -21.5 ‰ (MacDonald et al., 1991).

Previous work in Bute Inlet has used a wider range of methods (e.g. radiocarbon $\Delta^{14}C$ dating and separation of OC mixtures by ramped pyrolysis-oxidation RPO) on selected river and sandy channel samples (Hage et al., 2020). We complement these previous detailed measurements with new 14C and RPO measurements on three samples from the distal sub-environment (Fig. 7). The RPO method identifies POC fractions based on thermal lability by heating each sample from 20 to 1000 °C in an oxygenated carrier gas, thus sequentially combusting POC into CO_2. The CO_2 collected between temperature intervals ("fractions") is measured for carbon stable isotopes ($\delta^{13}C$) and radiocarbon activity ($^{14}C/^{12}C$). These isotope measurements on separated fractions enabled characterization of the distribution of POC source and age within individual samples (Hemingway et al., 2017).

3.4 Calculation of river organic carbon (OC) fluxes

In order to determine the particulate OC fluxes from rivers, we use bedload sediment discharge data published in past literature (Syvitski and Farrow, 1983, Text S2), recent total suspended sediment measurements conducted on the Homathko and Southgate Rivers (Text S3), and TOC measurements of river sediments collected in October 2017 (Table 1).

Bedload discharge for the Homathko River was estimated at 3100 Kt/yr by Syvitski and Farrow (1983). We scaled this Homathko bedload estimate to the Southgate River using the ratio of watershed areas (Table 1; Text S2). The yearly mean suspended load discharge for the Homathko and Southgate Rivers was estimated at 946 Kt/yr and 220 Kt/yr, respectively. This is based on suspended samples collected approximately monthly between 2018 and 2021 for the Homathko River (Text S3), together with daily water discharge data (Runkel et al. 2004; Text S3). There was no water discharge data available for the Southgate River up to 2021. Therefore, a linear regression was used to estimate daily Southgate River water discharge from Homathko River discharge, similar to Hood et al. (2020). The training dataset contained 123 daily flow observations spanning a broad range of flows from record high discharge in late June 2021 through moderately low flows in October 2021 (Text S1).

Finally, we derived both river OC fluxes by multiplying the average TOC between river bedload and suspended load samples with the annual bedload and suspended load discharge, respectively (Table 1).

3.5 Calculation of organic carbon burial rates in fjord sediments

The OC burial rates (kt/yr) in the fjord are calculated using Equation 1 (Table 2; Baudin et al., 2020) as follows:

$$A * TOC * \rho * (1- \varphi) * SR. \quad \text{(Equation 1)}$$

Where A is the surface area of a sub-environment (m^2), TOC is the total OC content (%) averaged between samples from a given sub-environment, ρ is the sediment density (kg/m^3), φ is the porosity (%), and SR is the sedimentation rate (m/yr).

Sedimentations rates (SRs) typically vary when measured over different timescales (Sadler, 1981), especially in a highly active turbidity current system (Prior et al., 1987, Heijnen et al., 2020), making them challenging to quantify. Thus, SRs were estimated herein based on two independent approaches that provide ranges of SRs (Texts S4 and S5). The first approach uses differences between two bathymetric surveys obtained in 2008 and 2018

and thus holds for a decennial timescale (Heijnen et al., in review, Table 2, Text S4). The second approach uses ^{210}Pb and ^{137}Cs dating methods applied to sediment cores collected in overbank and distal flat basin settings (Syvitski et al., 1988; Heerema, 2021; Text S5), and thus holds for a centennial timescale. Based on these two approaches and timescales, we use ranges of SRs for each sub-environment as follows. SR in the channel ranges from -16 cm/yr (i.e. erosional) to 0.7 cm/yr (i.e. slightly depositional). SR in the lobe ranges from 10 to 18 cm/yr, implying a large accumulation of sediment over both decennial and centennial timescales. SR in the overbank area varies between 2 to 2.3 cm/yr. Finally, SR in the distal flat basin ranges from 1 to 2.3 cm/yr.

We note that the first approach (i.e., 11 yr time-lapse bathymetric analysis) highlights zones of erosion and deposition that migrate upstream significantly (100 to 450 m per year) due to the presence of active knickpoints in the channel (Heijnen et al., 2020). This explains why the channel is net-erosive on a decennial timescale (SR = ~ -16 cm/yr). The 30 cm long sediment cores used in this study thus probably represent deposits that were a few days to weeks old, as direct monitoring shows that over 100 turbidity currents can occur in one freshet (Chen et al., 2021; Pope et al., in review). The top of these deposits were likely reworked again by turbidity currents in the following days to weeks, progressively moving the sediment down the channel. The channel thus acts as a conduit through which sand and associated OC is shuffled to the lobe, in multiple stages over several weeks to several decades (Heijnen et al., in review). Time-lapse bathymetry also shows that the terminal lobe is built up from a small number of large magnitude 'channel flushing' events (Heijnen et al., in review), resulting in a locally high SR (SR = 18 cm/yr, Table 2) over decennial timescales. It should be kept in mind that this bathymetric method underestimates the depositional volume in areas of slow deposition (overbanks), as cm-thin drapes of sediment cannot be resolved by this method. The second approach (i.e., ^{210}Pb and ^{137}Cs dating) postulates that the entire Bute submarine system is net aggrading over centennial timescales (Syvitski et al., 1988). Thus, the channel floor is assumed to aggrade at the same rate as the adjacent overbank areas, rather than being strongly erosional. This is consistent with a rather shallow (~20 m relief) channel, as prolonged erosion in a submarine channel that is likely at least hundreds of years old would

have carved a much deeper conduit. This assumption of overall aggradation results in a slow, but positive, SR in the channel (SR = 0.07 cm/yr). This SR in the channel is then assumed to be balanced by less aggradation in the lobe (SR = 10 cm/yr), such that the total sediment budget within the various sub-environments on the fjord seafloor then balances the rate at which sediment is supplied by the rivers (Table 1).

In total, all OC burial rates in the submarine system are provided as ranges (Table 2) based on the two approaches used to estimate SR.

	Channel floor		Lobe		Overbank		Distal basin		Total submarine system	
	10 yr	*100 yr*	*10 yr*	*100 yr*	*10 yr*	*100 yr*	*10 yr*	*100 yr*	*10 yr*	*100 yr*
Surface area (m^2)	12.2×10^6		15.4×10^6		77.0×10^6		58.0×10^6		163×10^6	
Sedimentation rate (m/yr)	-0.16[a]	0.007[b]	0.18[a]	0.1[b]	0.023[a]	0.02[c]	0.023[a]	0.01[c]		
Sedimentation rate error (m/yr)	-0.09	0.005	0.22	0.050	0.006	0.015	0.006	0.003		
Sediment volume budget (Mm^3/yr)	**-2.0[a]**	**0.1**	**2.73[a]**	**1.5**	**1.8**	**1.5**	**1.3**	**0.6**	**3.8**	**3.7**
Sediment volume budget error (Mm^3/yr)	-1.09	0.06	3.45	0.8	0.46	1.1	0.35	0.17	3.2	2.2
% coarse sand	63		63		7		0			
% fine sand	29		29		13		0			
% grey mud	8		8		80		65			
% red mud	0		0		0		35			
TOC in coarse sand (%)	0.03		0.03		0.04		0			
TOC in fine sand (%)	3.2		3.2		0.3		0			
TOC in grey mud (%)	0.5		0.5		0.3		0.7			
TOC in red mud (%)	0		0		0		2.5			
TOC weighted with facies (%)	1		1		0.3		1.3			
Porosity (%)	70		70		80		85			
Sediment density (kg/m^3)	2585		2585		2585		2585			
OC flux (Kt OC/yr)	**-15.6**	**0.7**	**21.2**	**11.9**	**2.9**	**2.4**	**6.8**	**2.9**	**15.4**	**17.9**
OC flux error (Kt OC/yr)	-8.5	0.5	26.9	5.9	0.8	1.7	1.2	0.9	20.3	9.1
Terrestrial OC flux (Kt OC/yr)	**-15.6**	**0.7**	**21.2**	**11.9**	**2.9**	**2.4**	**3.1**	**1.3**	**11.7**	**16.3**
Terrestrial OC flux error (Kt OC/yr)	-8.5	0.5	26.9	6.0	0.8	1.8	1.2	0.6	20.3	8.8
							Burial efficiency (%)		**50**	**70**

Table 2*: Sediment budget and organic carbon (OC) fluxes in the sub-environments of the Bute turbidite system over 10 and 100 yr timescales. a: sediment volumes derived from repeated bathymetric surveys between 2008 and 2018 (Heijnen et al.. in review). Sedimentation rates are obtained by dividing the sediment volume by the surface area of a given sub-environment. Volume uncertainties are based on vertical accuracy of the multibeam surveys of 0.5 % of the water depth. hence the 600 m deep lobe is greatly affected (Heijnen et al.. 2020). b: Assumed sedimentation rates in the channel and lobe are based on c and Baudin et al. (2020; see Suppl. Material). c: Sedimentation rates in the overbank and distal basin are based on 210Pb and 137Cs dating (Syvistki et al.. 1988. Heerema. 2020; Suppl. Material). OC annual fluxes are obtained as follows: OC flux = Sediment volume x TOC x (1-Porosity) x Density*

4 Results

Below we provide the OC content and composition for both rivers and the fjord sediments separately. We note that comparison between TC and TOC on all samples revealed the absence of carbonates within both river and fjord samples (Fig. 4).

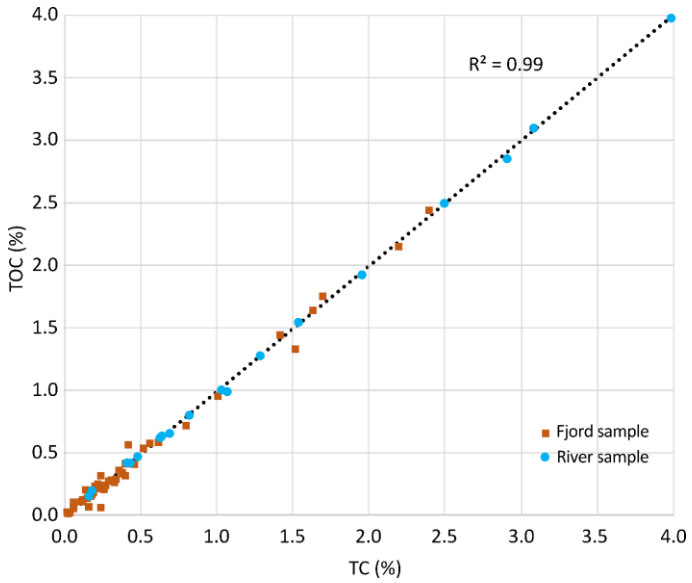

***Figure 4**: comparison between total carbon (including inorganic and organic carbon) and total organic carbon content measured on all samples collected in rivers and fjord.*

4.1 Carbon composition supplied by both rivers; what is coming in?

Coarse sand samples collected from the riverbank and delta areas have relatively low TOC (mean TOC = 0.35 %), and δ13C values (-27 to -28 ‰) indicating a terrestrial origin (Hecky and Hesslein, 1995). TOC is moderately high (mean TOC = 0.8 %) in the fine sands collected in the river waters, banks and deltas; whereas $\delta^{13}C$ values are low (-25 to -29 ‰) and point again to a terrestrial origin (Hecky and Hesslein, 1995). TOC is highest in muddy sediments (mean TOC = 3.1%, Fig. 5) collected in the river plume at the fjord head. $\delta^{13}C$ signatures for these river plume samples are unusually high (-12 to -20 ‰; Fig. 6), despite the absence of carbonates (Fig. 4). These

high $\delta^{13}C$ values are interpreted to be linked to bacterioplankton producing extra cellular polymeric substances (EPS; Albright, 1983), and this will be further discussed in Section 5.1.

In total, we estimate that about 23.4 ± 5.2 Kt OC/yr are delivered annually by the Homathko and Southgate Rivers. This is based on the estimated sediment discharge (suspended and bedload) and on the average TOC content measured between samples collected in both rivers in October 2017 (Table 1).

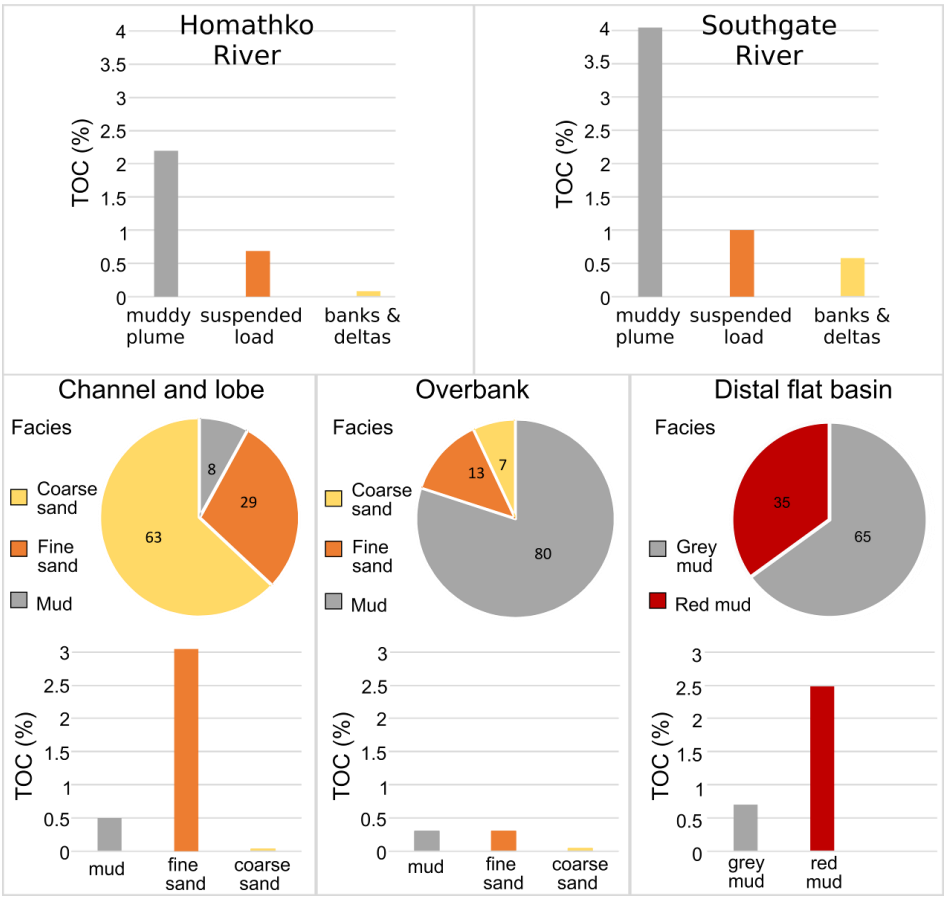

***Figure 5**: Facies and total organic carbon (TOC) content within rivers, submarine channel and lobe, overbank, and distal flat basin. Pie charts represent the contribution (in %) of each of the facies to a given sub-environment.*

4.2 Facies and carbon composition in the fjord; what is preserved and where?

We now present the OC content and composition within the fjord seabed, across the four previously-defined sub-environments (Fig. 3).

Sediment cores collected from the sandy channel floor and lobe have similar facies and OC composition, thus the OC composition of these sub-environments are described together. The channel floor and lobe contain 63 % carbon-poor (mean TOC = <0.05 %) coarse sand; 29% of carbon-rich (mean TOC = 3 %) fine sand; and 8 % of carbon-moderate (mean TOC = 0.5 %) mud (Fig. 5). $\delta^{13}C$ and ^{14}C ages revealed that fine sands contain young terrestrial woody debris (visible to the naked eye), buried under older biospheric soil organic matter in the muds (Hage et al., 2020; Fig. 6).
In contrast to the channel floor and lobe, the overbanks are dominated (80 %) by muddy deposits characterized by lower TOC values (0.35 % on average; Fig. 5). Fine sands found in the overbank cores have much lower TOC values compared to fine-sands in the channel floor and lobe. δ13C signatures range between -26 and -28 ‰, pointing to a terrestrial origin of the organic matter (Fig. 6). We note the absence of woody debris visible to the naked eye in the overbank cores, as opposed to the channel floor and lobe cores.

The top two meters of sediment recovered from the distal flat basin is made exclusively of muddy sediments characterized by a homogenous red (35 %) or grey facies (65 %). Grey muds have moderate TOC (0.65 % on average; Fig. 5) and a wide range of $\delta^{13}C$ signatures, suggesting a mixed terrestrial and marine origin of organic matter (-22 to -26 ‰; Fig. 6). Red muds have high TOC (2.5 % on average; Fig. 5) with $\delta^{13}C$ between -20.5 and -23 ‰ (Fig. 6) that point to a marine-dominated origin (MacDonald et al., 1991). Based on a binary mixing model using $\delta^{13}C$ compositions of marine and terrestrial OC end-members, we estimate that about 54 % of the organic carbon found in the upper two meter sediment of the distal flat basin is of

marine origin (Text S6, Table S6). ^{14}C data and RPO thermograms on the red and grey muds in this distal site (Fig. 7) reveal that the OC in this muddy distal site is of similar age (500 to 1100 ^{14}C yr), compared to the organic matter found in the muddy deposits of the channel (997 ^{14}C yr; Fig. 6). Overall, OC associated with muds in the active channel and distal flat basin are older compared to the young OC associated fine sands found in the active channel (Fig. 6, Hage et al., 2020), due to mineral protection of old biospheric OC in muddy sediments (Hemingway et al., 2019).

In total, we estimate that the top two meters of sediments in the Bute turbidity current system comprise an annual OC burial rate ranging from 15.4 to 17.9 Kt OC/yr over decennial to centennial timescales, respectively (Table 2). We divide this budget between terrestrial and marine organic carbon contribution based on the mixing model applied to the distal flat basin samples (Text S6). In total, between 11.7 and 16.3 Kt OC/yr of terrestrial origin carbon are found in the fjord, in all of its sub-environments. Between 1.6 and 3.7 Kt OC/yr of marine origin carbon are found in the distal flat basin (Figs. 6 and 7, Table 2).

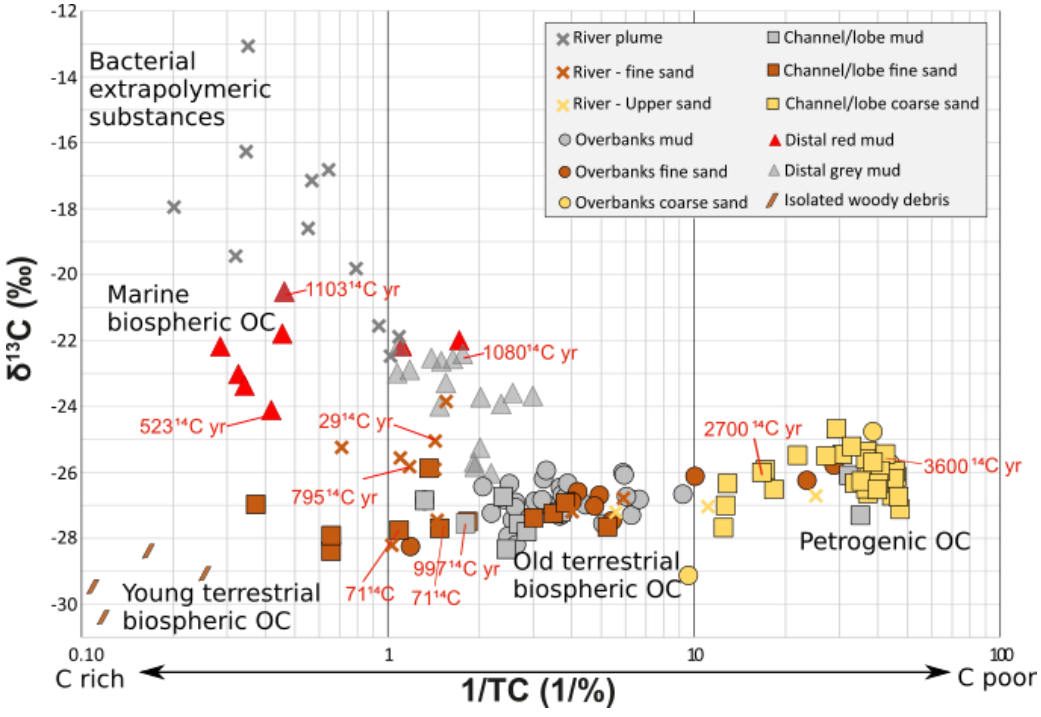

***Figure 6**: Total Carbon content (TC) versus carbon stable isotopes ($\delta^{13}C$) measured on all samples collected in the rivers and in the Bute turbidity current system. $\delta^{13}C$ values are reported relative to Vienna Pee-Dee Belemnite (VDBP). Radiocarbon dates are expressed as reservoir age offsets in ^{14}C years (following Soulet et al., 2016). The combination of bulk measurement of carbon, stable isotopes and radiocarbon isotopes allowed five carbon pools to be identified. (1) Extra polymeric substances associated with bacterioplankton in the river plumes at the surface of the fjord waters (Albright, 1983). (2) Marine carbon produced in the distal site. (3) Young terrestrial carbon in the form of woody debris almost exclusively buried in the sandy submarine channel. (4) Old terrestrial biospheric organic carbon aged in soils. (5) Petrogenic (rock-derived) organic carbon associated with coarse sand.*

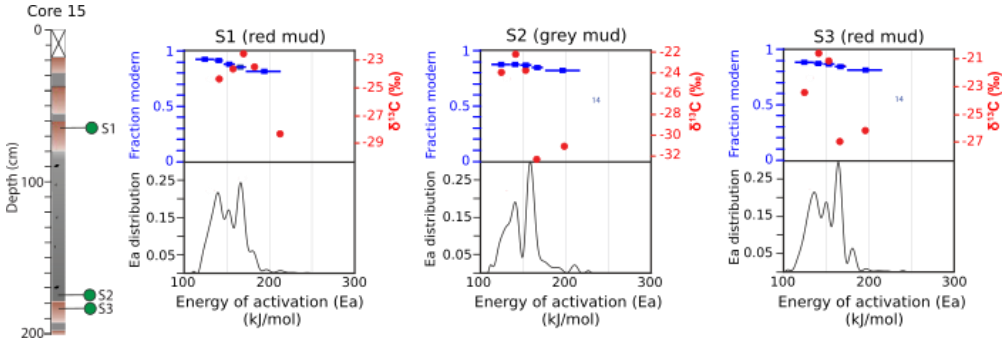

***Figure 7**: Separation of OC mixtures by ramped oxidation (RPO) for three samples collected in the distal flat basin (Core 15 in Fig. 3). Two facies are identified in this core: muddy sediment with a reddish colour and muddy sediments with a grey colour and organic debris. Black lines show distribution of activation energy (Ea) (thermogram; Hemingway et al., 2017). Blue squares show radiocarbon ages (in fraction modern, Fm, a measurement of the deviation of the $^{14}C/^{12}C$ ratio of a carbon fraction from "modern"). Red dots show carbon stable isotopes ($\delta^{13}C$, in ‰). Blue bars represent the Ea range to which each red dot and blue square applies.*

5 Discussion

5.1 How much particulate organic carbon is delivered by the two rivers discharging into Bute Inlet?

We have estimated that Homathko and Southgate Rivers carried 23 ± 5 Kt OC/yr into Bute Inlet based on suspended and bedload sampling conducted in 2017 (Table 1). This total OC flux is interpreted to contain three pools (Fig. 6): young terrestrial biospheric (woody debris); old terrestrial biospheric (soil organic matter); and petrogenic OC (rock-derived OC).

Identification of these pools is based on TOC and $\delta^{13}C$ signatures (Fig. 6), and on ramped oxidation data combined with radiocarbon dates previously presented in Hage et al. (2020). To these three pools previously identified, we add a fourth pool made of extracellular polymeric substances (EPS) associated with bacterioplankton that occurs when the rivers enter the fjord and create surface plumes in which the heterotrophic activity of bacterioplankton can be enhanced (Albright, 1983). This activity appears to result in an OC pool characterized by high TOC (>3 %) and unusually high $\delta^{13}C$ signatures (Fig. 6). Such signatures cannot be explained by the presence of carbonates (typically enriched in $\delta^{13}C$) because they were removed prior to isotope measurements. These high $\delta^{13}C$ signatures may also correspond to C4 plants, yet C4 plants are almost exclusively found in tropical and warm environments (Hecky and Hesslein, 1995). Instead, we suggest that the high TOC and associated $\delta^{13}C$ signatures correspond to bacterial extracellular polymeric substances (EPS). The EPS hypothesis is further supported by the stickiness of the plume samples, which is typical for EPS (Underwood et al., 1995). This fourth pool of OC is not included in our OC river input flux as it is most likely formed within the fjord water. Further research on the highly enriched $\delta^{13}C$ composition of these plume samples is required, yet it is beyond the scope of this study. We further note that the EPS-related OC pool is not found in the fjord seabed sediment samples (Fig. 6). We propose this is because OC associated with EPS is labile and not heavy enough to settle, and it thus degrades rapidly in the water column before reaching seabed sediments (Albright, 1983).

We note that there are key assumptions behind these estimates of riverine OC composition. First, we have a limited number of river samples (n=22) and these samples were collected during a rain-induced runoff event in fall when river discharge was near the annual average (Text S1). River discharge peaks driven by the freshet and/or intense rain likely brought more and coarser terrestrial organic debris than the rates estimated here (as in Turowski et al., 2016). We thus expect these river OC fluxes to fluctuate not only seasonally but also following extreme events such as floods and intense rain, yet the data presented in this study do not constrain this variability. Second, we have no constraints on the OC content potentially coming from small streams entering the fjord along its margins. However,

these streams only represent 6 % of the total sediment and freshwater input coming into the fjord (Syvitski and Farrow, 1983).

5.2 How much and what type of organic is buried in the Bute Inlet sub-environments?

The surficial sediments from the Bute turbidity current system bury a total of 15.4 – 17.9 Kt OC/yr, with 11.7 to 16.3 Kt OC/yr being of terrestrial origin. 76 to 91 % of the OC buried in Bute Inlet is thus terrestrial. This proportion is higher compared to previous estimates made in other fjords where 42 to 65 % of the OC was found to be terrestrial (Cui et al., 2016, Smeaton & Austin, 2020). This further highlights the importance of turbidity currents for distributing terrestrial OC in river-fed fjords, and the necessity to include turbidity current processes when assessing the burial of terrestrial OC globally.

There are a number of uncertainties behind OC fluxes calculated in Bute Inlet. First, we do not have sediment cores in the external parts of the overbanks, close to the fjord's sidewalls. Therefore, we extrapolate the OC composition found in the overbanks close to the channel to the entire overbank area. These more distal sites in the overbank may either be poorer in terrestrial OC compared to the sites close to the channel fed by the rivers, or richer in OC due to smaller rivers and streams and potential landslides sourced from the fjord steep sidewalls. Second, we assume that the 30 cm thick (i.e. maximum a few weeks old) deposits recovered from the channel are reproduced over centennial timescales despite the rapidly migrating knickpoints in the channel (Prior et al., 1987, Heijnen et al., 2020). We could expect that channel-floor fine sands, which are rich in OC, are excavated several times before reaching their ultimate burial location on the lobe, decreasing their OC content over time (Heijnen et al., in review). However, we do not see any evidence of OC content decrease along the channel transect, at least over the very recent (30 cm below seafloor) deposits observed in this study. We suspect that the channel is an efficient conduit for the delivery of terrestrial OC to the lobe, but this needs to be confirmed with longer sediment cores that are difficult to collect in sandy channel floors (as piston corers tend to fail to penetrate sandy seabed).

Despite these uncertainties, the data collected in Bute Inlet allow us to derive for the first time a detailed OC burial budget in fjord sediments controlled by turbidity currents (Fig. 8). Together the channel and lobe, dominated by sands (Fig. 5) and only covering 17 % of the fjord's seafloor area, comprise 48 to 77 % of the total annual terrestrial OC burial flux in Bute Inlet. This terrestrial OC is predominantly young, associated with fine sands and buried beneath a layer of mud (Hage et al., 2020, Fig. 6). The overbanks, dominated by mud (Fig. 5) and covering 47 % of the fjord's seafloor area, comprise 15 to 25 % of the total annual terrestrial OC burial flux, with low TOC in the fine sands. The settling velocities of waterlogged woody debris have been shown to be relatively rapid due to their size and density (Waterson et al., 2008, Hoover et al., 2010, McArthur et al., 2016), such that this woody debris is carried mainly along the channel floor. This concentration of woody debris along the channel floor could explain the low TOC values seen within the fine-sands of the overbanks. The distal flat basin, exclusively made of mud in the surficial (200 cm) sediment and covering 36 % of the fjord's seafloor area, comprises the remaining 6 to 22 % of the total annual terrestrial OC burial flux. The abundance of mud in the surficial sediment of the distal flat basin is explained by the limited number of turbidity currents reaching this site in present times (Prior et al., 1987; Chen et al., 2021; Pope et al., in review).

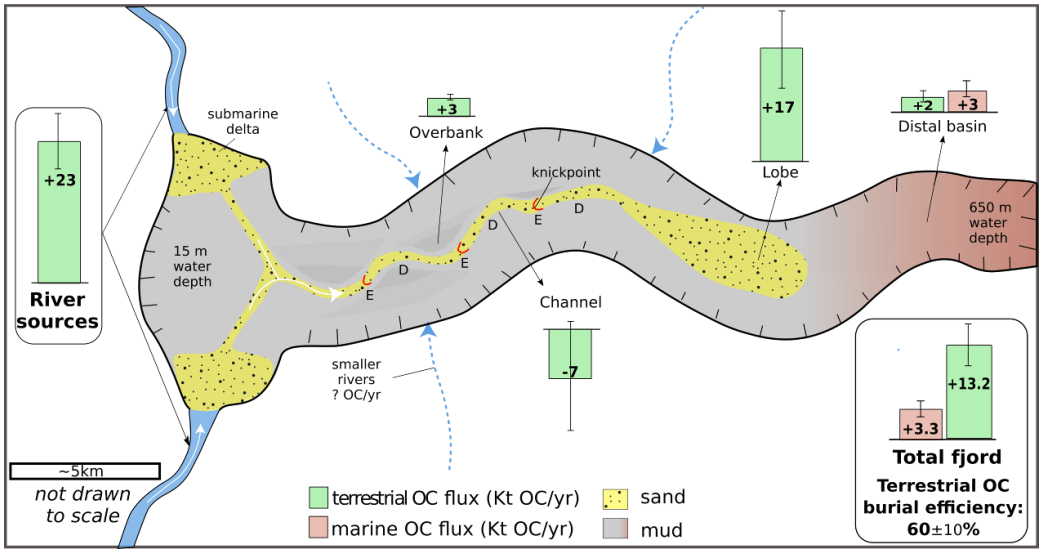

***Figure 8**: Summary illustration (not to scale) showing total organic carbon (OC) fluxes from rivers to seafloor sediment in Bute Inlet. OC fluxes are given as the average value between sediment budgets estimated using two approaches (see Methods; Heijnen et al., in review, Syvitski et al., 1988, Heerema, 2021). Error bars*

correspond to the range between the two approaches. Sediment and OC are shuffled stepwise down the channel before reaching the lobe due to migrating knickpoints. The channel is thus net erosive over decennial timescales, with patches of erosion (E) and deposition (D) between knickpoints. Over longer timescales (>100's yr), the channel is interpreted as being neutral to slowly aggrading.

5.3 What is the terrestrial OC burial efficiency of Bute Inlet and how does it compare with other fjords?

Comparison between OC river input (23 ± 5 Kt OC/yr) and terrestrial OC burial rate in Bute Inlet (11.7 to 16.3 Kt OC/yr), suggests that Bute Inlet has a terrestrial OC burial efficiency ranging between 50 and 70 % (60 ± 11 % on average) when estimated over decennial and centennial timescales, respectively.

No study has closed budgets between river sources and fjord sediments before, so it is not possible to compare this value with other river-fed fjords. However, we can compare our results in Bute Inlet with previous fjord studies, by normalizing OC burial rates to the Bute Inlet's total surface area. By doing so, the burial of terrestrial OC in Bute Inlet ranges between 72 and 100 t C/km^2/yr. This range lies between previous estimates of OC fluxes of 57 to 107 t C/km^2/yr in Scottish and Irish fjords that were described as having heterogeneous seafloors (Smeaton and Austin, 2020). Importantly, our results from Bute Inlet suggest that fjords characterised by sandy turbidity current systems may bury over three times more terrestrial OC compared to previous global estimates based on muddy cores from fjords without any identified turbidity current channels (22 t C/km^2/yr; Smith et al., 2015, Cui et al., 2016).

5.4 Comparison with larger, deep-sea turbidity current systems

To our knowledge, only one study has provided OC balance budgets between river source and turbidity current sub-environments within a single system. This is the Congo River to deep-sea Fan (Baudin et al., 2020), where burial rates are calculated over centennial timescales that are comparable to the longer timescales considered in this study. Using a source to sink approach, Baudin et al. (2020) found that 33 to 69 % of the annual OC delivered by

the Congo River is buried in the Congo turbidity current system. This burial efficiency is similar to, if slightly lower than, our estimate in Bute Inlet (50 to 70 %), highlighting the difficulty in closing budgets between river source and marine sinks fed by turbidity currents, particularly in open marine systems such as the Congo system (Baudin et al., 2020). Within these two turbidity current systems, both the Congo and Bute Inlet submarine canyon-channels show minimal long-term (> 100 year) OC accumulation (Fig. 8, Baudin et al., 2020). We note however that under-sampling of the Congo Canyon and Channel occurred in past studies due to the difficulty with sampling sandy deposits (Baudin et al., 2020). This under-sampling of the canyon and channel may result in underestimation of OC burial rates in the Congo Channel, similarly to the Bute Inlet channel where only 30 cm long sediment cores could be retrieved. In both Congo and Bute Inlet systems, the lobe holds most of the total buried OC.

Besides this example from the Congo system, work in Gaoping Canyon offshore Taiwan shows a terrestrial OC preservation efficiency of > 70% in marine sediments. The Gaoping submarine canyon is supplied by river floods (hyperpycnal) and dilute surface plumes (hypopycnal) inputs (Kao et al., 2014). This high OC burial efficiency results from this mountainous island being a hotspot for sediment and OC production, with frequent typhoons that deliver terrestrial OC (e.g. woody debris associated with sands) through the submarine canyon to the deep-sea (Hilton et al., 2008, West et al., 2011, Liu et al., 2016). Another example of high OC burial efficiency comes from the Bay of Bengal where almost no loss of OC was observed between the Ganges-Brahmaputra River inputs and the Bengal Submarine Fan (Galy et al., 2007). Coarse turbidity current deposits from the channel-levees of the Bengal Fan submarine system were also shown to have abundant terrestrial woody fragments throughout the last 19 My (Lee et al., 2019). These OC-rich turbidity current deposits are interpreted to result from high-magnitude, low-frequency events (e.g. floods, cyclones; Lee et al.; 2019).

Based on these examples, it is plausible that rare and extreme events may also affect the OC burial efficiency and distribution in Bute Inlet. It was recently shown that most turbidity currents (~90 %) dissipate within the shallowest-water (< 200 m depth and < 12 km along channel from the delta) part of Bute Inlet, whereas less frequent (~10%) events rework this material

and progressively shuffle it downstream to the lobe (Heijnen et al., in review). We further suspect that rare long runout events can flush material to the distal flat basin, as evidenced by thick sandy accumulations found at >3 m depth in 8 m long piston cores collected in the distal basin at the location of core 15 (Fig. 3, Heerema, 2021). Based on our OC burial efficiency estimates (i.e., 50 to 70 % over decennial to centennial timescales, respectively), it appears that OC burial efficiency is higher when considering longer timescales, which are more likely to integrate some large events than shorter timescales.

An example of rare and large event occurred in the Bute Inlet area on 28 November 2020 when a glacial lake outburst flood took place at Elliot Creek, which is a tributary of Southgate River (Fig. 1). This outburst flood caused an exceptionally large landslide involving 15 million cubic meters of terrestrial material, some of which was released into the Southgate River, ultimately discharging into Bute Inlet (Geertsema et al., in review, https://blogs.agu.org/landslideblog/2020/12/16/bute-inlet-landslide/). The impact of this event on the OC burial in Bute Inlet is yet to be determined and compared with the pre-event OC fluxes presented in this study, but it may help to understand sediment and OC delivery in most infrequent but large magnitude events.

6 Conclusion

This study provides the first complete source-to-sink budget for organic carbon (OC) in a river-fed fjord turbidity current system, showing how OC is distributed within the upper <2 m of sediment. OC fluxes are estimated for the fjord's two river sources (Homathko and Southgate Rivers, which provide 94 % of the water and sediment discharge to the fjord), and compared to OC burial fluxes in different seafloor sub-environments. We estimate that the annual OC export from both rivers to the fjord is 23 ± 5 Kt C/yr, although this may not capture the full annual range of streamflow variability. The annual terrestrial OC burial rate of the entire fjord is estimated to range from 12 to 16 Kt OC/yr. This suggests that a relatively high terrestrial OC burial efficiency (60 ± 10 %) occurs within the fjord. Terrestrial OC is distributed as follows across the fjord seafloor; 63 ± 14 % of the total terrestrial OC burial occurs in the sand-dominated channel floor and lobe (covering 17 % of the fjord seafloor area), whereas 37 ± 14 % occurs

in the mud-dominated overbank and distal flat basin (covering 83 % of the fjord seafloor area). Therefore, hydrodynamic fractionation of OC by turbidity currents leads to variable burial efficiencies in different sub-environments of the fjord. This study helps to understand how OC is buried within fjords over short (decennial to centennial) timescales. A comparison to other (non-fjord) turbidity current systems suggests that these systems consistently have high (50 to 100 %) terrestrial OC burial efficiency (Galy et al., 2007, Liu et al., 2016, Hilton et al., 2017; Baudin et al., 2020). Turbidity current systems may thus play a globally important role in the highly efficient delivery and burial of mainly terrestrial OC, which affects atmospheric CO_2 levels over geological timescales (Berner, 1982) and food resources for modern benthic ecosystems (Włodarska-Kowalczuk et al., 2019).

Data availability: Discharge data for the Homathko River and Southgate River are available from https://wateroffice.ec.gc.ca; station 08GD004 and station 08GD010, respectively. Multibeam bathymetric data are held by the Geological Survey of Canada and Canadian Hydrographic Survey. Sediment core and river sample locations are provided in the supplementary material of this study, as well as organic geochemistry measurements made on each sample (Tables S1, S2, S7 and S8).

7 Acknowledgements

We acknowledge that this work took place in the unceded traditional territory of the Homalco First Nation. We thank the captain and crew of the CCGS Vector (Canada) for sample collection. S.H. acknowledges funding by the IAS postgraduate grant scheme, a Research Development funds offered by Durham University, and the NOCS/WHOI exchange program. S.H. has received funding from the European Union's Horizon 2020 research and innovation programme under the Marie Sklodowska-Curie grant agreement No 899546. The field campaign and geochemical analyses were supported by Natural Environment Research Council Grants NE/M007138/1, NE/W30601/1 and NE/M017540/1. M.J.B.C. was funded by a Royal Society Research Fellowship (DHF\R1\180166). M.A.C. was supported by the U.K. National Capability NERC CLASS program (NE/R015953/1) and NERC Grants (NE/P009190/1 and NE/P005780/1). C.J.H. and M.S.H. were funded by the European Union's Horizon 2020 research and innovation program under the Marie Skłodowska- Curie grant agreement No. 721403 - ITN SLATE. E.L.P. was supported by a Leverhulme Early Career Fellowship (ECF-2018-267).

8 References

1. Albright, L. J. (1983). Influence of river-ocean plumes upon bacterioplankton production of the Strait of Georgia, British Columbia. *Marine Ecology - Progress Series*, 12, 107-113.
2. Baudin, F., Martinez, P., Dennielou, B., Charlier, K., Marsset, T., Droz, L., & Rabouille, C. (2017). Organic carbon accumulation in modern sediments of the Angola basin influenced by the Congo deep sea fan. *Deep-Sea Research Part II*, 142, 64-74.

3. Baudin, F., Rabouille, C., & Dennielou, B. (2020). Routing of terrestrial organic matter from the Congo River to the ultimate sink in the abyss: a mass balance approach (André Dumont medallist lecture 2017). *Geologica Belgica*, 23(1-2).
4. Berner, R. A. (1982). Burial of organic carbon and pyrite sulfur in the modern ocean: its geochemical and environmental significance. *American Journal of Science, 282*, 451-473. doi:10.2475/ajs.282.4.451
5. Berner, R. A. (1989), Biogeochemical cycles of carbon and sulfur and their effect on atmospheric oxygen over Phanerozoic time, *Paleogeogr. Paleoclimatol. Paleoecol.*, 75, 97–122.
6. Bianchi, T.S., Arndt, S., Austin, W.E.N., Benn, D.I., Bertrand, S., Cui, X., Faust, J. C., Koziorowska-Makuch, K., Moy, C.M., Savage, C., Smeaton, C., Smith, R.W., Syvitski, J. 2020. Fjords as Aquatic Critical Zones (ACZs). *Earth-Science Reviews* (203), pp. 103-145. doi: 10.1016/j.earscirev.2020.103145.
7. Bornhold, B. D., Ren, P., & Prior, D. B. (1994). High-frequency turbidity currents in British Columbia fjords. *Geo-Marine Letters, 14*, 238-243.
8. Burdige, D. J. (2005). Burial of Terrestrial Organic Matter in Marine Sediments: A Re-Assessment. *Global Biogeochemical Cycles, 19*(7). doi:10.1029/2004gb002368
9. Burdige, D. J. (2007). Preservation of organic matter in marine sediments: controls, mechanisms, and an imbalance in sediment organic carbon budgets? *Chemical Reviews, 107*, 467-485. doi:10.1021/cr050347q
10. Chen, Y., Parsons, D.R., Simmons, S.M., Williams, R., Cartugny, M.J.B., Hughes Clarke, J.E., Stacey, C.D., Hage, S., Talling, P.J., Azpiroz-Zabala, M.A., Clare, M.A., Hizzett, J.L., Heijnen, M.S., Hunt, J.E., Lintern, D.G., Sumner, E.J., Vellinga, A.J., Vendettuoli, D. (2021). Knickpoints and crescentic bedform interactions in submarine channels. *Sedimentology, 68*, 1358-1377
11. Cui, X., Bianchi, T. S., Savage, C., Smith, R.W. (2016) Organic carbon burial in fjords: terrestrial versus marine inputs. *Earth and Planetary Science Letters, 451*, 41-50.
12. Cui, X., Bianchi, T. S., Jaeger, J. M., & Smith, R. W. (2016). Biospheric and petrogenic organic carbon flux along southeast Alaska. *Earth and Planetary Science Letters, 452*, 238-246.

13. Cui, X., Bianchi, T. S., & Savage, C. (2017). Erosion of modern terrestrial organic matter as a major component of sediments in fjords. *Geophysical Research Letters*, 44, 1457–1465.
14. Conway, K. W., Barrie, J. V., Picard, K. & Bornhold, B. D. (2012). Submarine channel evolution: active channels in fjords, British Columbia, Canada. *Geo-Marine Letters,* 32, 301–312.
15. Coynel, A., Seyler, P., Etcheber, H., Meybeck, M., & Orange, D. (2005). Spatial and seasonal dynamics of total suspended sediment and organic carbon species in the Congo River. *Global Biogeochemical Cycles*, 19(4). doi:10.1029/2004gb002335
16. Decho, A. W., & Gutierrez, T. (2017). Microbial Extracellular Polymeric Substances (EPSs) in Ocean Systems. *Frontiers in Microbiology*, 8(922). doi:10.3389/fmicb.2017.00922
17. Deptuck, M. E., Sylvester, Z., Pirmez, C., O'Byrne, C. Migration-aggradation history and 3-D seismic geomorphology of submarine channels in the Pleistocene Benin-major Canyon, western Niger Delta slope. 2007. *Marine and Petroleum Geology, 24, 406-433.* doi:10.1016/j.marpetgeo.2007.01.005
18. Dyer, K. R. (1997). Estuaries: A Physical Introduction. New York, NY.
19. Farrow, G. E., Syvitski, J. P. M., & Tunnecliffe, V. (1983). Suspended particulate loading on the macro-benthos in a highly turbid fjord; Knight Inlet, British Columbia. *Canadian Journal of Fisheries and Aquatic Science, 40*(1), 273-288.
20. Gaines, S. M., Eglinton, G., & Rullkotter, J. (2009). Echoes of life: what fossil molecules reveal about earth history: Oxford University Press.
21. Gales, J. A., Talling, P. J., Cartigny, M. J., Hughes Clarke, J., Lintern, G., Stacey, C., & Clare, M. A. (2019). What controls submarine channel development and the morphology of deltas entering deep-water fjords? *Earth Surface Processes and Landforms,* 44(2), 535-551.
22. Galy, V. V., Peucker-Ehrenbrink, B., & Eglington, T. (2015). Global carbon export from the terrestrial biosphere controlled by erosion. *Nature Letter*, 521. doi:10.1038/nature14400
23. Geertsema, M. Menounos, B., Bullard, G., Carrivick, J.L., Clague, J.J., Dai, C., Donati, D., Ekstrom, G., Jackson, J.M., Lynett, P., Pichierri, M., Pon, A., Shugar, D.H., Stead, D., Del Bel Belluz, J., Friele, P., Giesbrecht, I., Heathfield, D., Millard, T., Nasonova, S., Schaeffer,

A.J., Ward, B.C., Blaney, D., Blaney, E., Brillon, C., Bunn, C., Floyd, W., Higman, B., Hughes, K.E., McInnes, W., Mukherjee, K., Sharp, M.A. (in review, Geophysical Research Letters). The 28 November 2020 landslide, tsunami, and outburst flood – a hazard cascade associated with rapid deglaciation at Elliot Creek, British Columbia, Canada.

24. Giesbrecht, I.J.W, Tank, S.E., Frazer, G.W., Hood, E.W., Gonzalez Arriola, S.G., Butman, D.E., D'Amore, D.V., Hutchinson, D., Bidlack, A., and Lertzman, K.P. (in press, Global Biogeochemical Cycles). Watershed classification predicts streamflow regime and organic carbon dynamics in the Northeast Pacific coastal temperate rainforest.
25. Gonzalez Arriola, S., Giesbrecht, I.J.W., Biles, F.E., and D'Amore, D.V. 2018. Watersheds of the northern Pacific coastal temperate rainforest margin. Hakai Institute Data Package. doi: 10.21966/1.715755
26. Hage, S., Cartigny, M. J. B., Sumner, E. J., Clare, M. A., Hughes Clarke, J. E., Talling, P. J., Lintern, D.G., Simmons, S.M., Silva Jacinto, R., Vellinga, A.J., Allin, J.R., Azpiroz-Zabala, M., Hales, J.A., Hizzett., J.L., Hunt, J.E., Mozzato, A., Parsons, D.R., Pope, E.L., Stavey, C.D., Symons, W.O., Vardy, M.E., Watts, C. (2019). Direct Monitoring Reveals Initiation of Turbidity Currents From Extremely Dilute River Plumes. *Geophysical Research Letters, 46*(20), 11310-11320. doi:10.1029/2019gl084526
27. Hage, S., Galy, V., Cartigny, M., Acikalin, S., Clare, M., Gröcke, D., Hilton, R.G., Hunt., J.E., Lintern, D.G., McGhee, C., Parsons., D.R., Stacey., C.D., Sumner, E.J., Talling. P.J. (2020). Efficient preservation of young terrestrial organic carbon in sandy turbidity-current deposits. *Geology*, 48 (9): 882–887.
28. Hecky, R.E. and Hesslein, R.H. Contributions of Benthic Algae to Lake Food Webs as Revealed by Stable Isotope Analysis (1995). *J. N. Am. Benthol. Soc.,* 14(4):631-653
29. Hedges, J. I., & Keil, R. G. (1995). Sedimentary organic matter preservation: an assessment and speculative synthesis. *Marine Chemistry, 49*(81e115). doi:10.1016/0304-4203(95)00008-F
30. Heerema, C. J. (2021). Evolution of Turbidity Currents: New insights from direct field measurements, Durham theses, Durham University. *Available at Durham E-Theses Online: http://etheses.dur.ac.uk/13963/*

31. Heijnen, M. S., Clare, M. A., Cartigny, M. J., Talling, P. J., Hage, S., Lintern, D. G., Stacey, C.D., Parsons, D.R., Simmons, S.M., Chen, Y., Sumner, E.J., Dix, J.K., Hughes Clarke, J.E. (2020). Rapidly-migrating and internally-generated knickpoints can control submarine channel evolution. *Nature communications*, 11(1), 1-15.
32. Heijnen, M. S., Clare, M.A., Cartigny, M. J., Talling, P.J., Hage, S., Pope, E.L., Bailey, L., Sumner, E.J., Lintern, D.G., Stacey, C.D., Parsons, D.P., Simmons, S.M., Chen, Y., Hubbard, S.M., Eggenhuisen, J.T., Kane, I., Hughes Clarke, J.E. (in review, EPSL) Fill, flush or shuffle: How is sediment carried through submarine channels to build lobes?
33. Hemingway, J. D., Rothman, D. H., Rosengard, S. Z., and Galy, V. V.: Technical note: An inverse method to relate organic carbon reactivity to isotope composition from serial oxidation, *Biogeosciences*, 14, 5099–5114, https://doi.org/10.5194/bg-14-5099-2017, 2017.
34. Hemingway, J.D., Rothman, D.H., Grant, K.E., Rosengard, S.Z., Eglington, T.I., Derry, L.A., Galy, V.V. 2019. Mineral protection regulates long-term global preservation of natural organic carbon. *Nature* 570, 228–231. https://doi.org/10.1038/s41586-019-1280-6
35. Hilton, R.G., West, A.J. Mountains, erosion and the carbon cycle. (2020). Nature Review Earth Environ 1, 284–299.
36. Hilton, R. G., Galy, A., Hovius, N., Chen, M. C., Horng, M. J., & Chen, H. (2008). Tropical-cyclone-driven erosion of the terrestrial biosphere from mountains. *Nature Geoscience*, 1(11), 759-762.
37. Hizzett, J. L., Hughes Clarke, J. E., Sumner, E. J., Cartigny, M. J. B., Talling, P. J., & Clare, M. A. (2018). Which triggers produce the most erosive, frequent, and longest runout turbidity currents on deltas? . *Geophysical Research Letters, 45*, 855-863.
38. Hoover, T.M., Marczak, L.B., Richardson, J.S. &Yonemitsu, N. (2010) Transport and settlement of organic matter in small streams. *Freshwater Biology*, 55(2), 436-449.
39. Hughes Clarke, J.E., Talling, P.J., Cartigny, M.J.C. (2015) Flow by flow monitoring within fjord-delta turbidite systems: Insights into deep water channel-to-lobe transitions. *American Geoscience Union annual meeting*, 2015

40. Hunter, W., Jamieson, A., Huvenne, V., & Witte, U. (2013). Sediment community responses to marine vs. terrigenous organic matter in a submarine canyon. *Biogeosciences*.
41. Kao, S.-J., Hilton, R.G., Selvaraj, K., Dai, M., Zehetner, F., Huang, J.-C., Hsu, S.-C., Sparkes, R., Liu, J.T., Lee, T.-Y., Yang, J.-Y. T., Galy, A., Xu, X., Hovius, N. (2014) Preservation of terrestrial organic carbon in marine sediments offshore Taiwan: mountain building and atmospheric carbon dioxide sequestration. *Earth Surface Dynamics*, 2, 127-139.
42. LaRowe, D. E., Arndt, S., Bradley, J. A., Estes, E. R., Hoarfrost, A., Lang, S. Q., Lloyd, K.G., Mahmoudi, N., Orsi, W.D., Shah Walter, S.R., Steen, A.D., Zhao, R. (2020). The fate of organic carbon in marine sediments-New insights from recent data and analysis. *Earth-Science Reviews*, 103146.
43. Lee, H., Galy, V., Fend, X., Ponton, C., G., A., France-Lanord, C., & Feakins, S. (2019). Sustained wood burial in the Bengal Fan over the last 29 million years. *Proceedings of the National Academy of Sciences of the United States of America, 116*(45), 22518-22525.
44. Liu, J. T., Hsu, R. T., Hung, J.-J., Chang, Y.-P., Wang, Y.-H., Rendle-Bühring, R. H., Yang, R. J. (2016). From the highest to the deepest: The Gaoping River–Gaoping Submarine Canyon dispersal system. *Earth-Science Reviews*, 153, 274-300.
45. Macdonald, R., Macdonald, D., O'Brien, M., & Gobeil, C. (1991). Accumulation of heavy metals (Pb, Zn, Cu, Cd), carbon and nitrogen in sediments from Strait of Georgia, BC, Canada. *Marine Chemistry*, 34(1-2), 109-135.
46. McArthur, A. D., Kneller, B. C., Wakefield, M. I., Souza, P. A., & Kuchle, J. (2016). Palynofacies classification of the depositional elements of confined turbidite systems: Examples from the Gres d'Annot, SE France. *Marine and Petroleum Geology*, 77, 1254-1273. doi:10.1016/j.marpetgeo.2016.08.020
47. McArthur, A., Kneller, B., Souza, P., & Kuchle, J. (2016). Characterization of deep-marine channel-levee complex architecture with palynofacies: An outcrop example from the Rosario Formation, Baja California, Mexico. *Marine and Petroleum Geology*, 73, 157-173.
48. McArthur, A., Gamberi, F., Kneller, B., Wakefield, M., Souza, P., & Kuchle, J. (2017). Palynofacies classification of submarine fan

depositional environments: Outcrop examples from the Marnoso-Arenacea Formation, Italy. *Marine and Petroleum Geology*, 88, 181-199.

49. Plink-Björklund, P., & Steel, R. J. (2004). Initiation of turbidity currents: outcrop evidence for Eocene hyperpycnal flow turbidites. *Sedimentary Geology*, 165(1-2), 29-52.
50. Pope, E. L., Normandeau, A., O Cofaigh, C., Stokes, C.R., Talling, P.J. 2019. Controls on the formation of turbidity current channels associated with marine-terminating glaciers and ice sheets. *Marine Geology* (415). doi: 10.1016/j.margeo.2019.05.010
51. Pope, E.L., Cartigny, M.J.B., Clare, M.A., Talling, P.J., Lintern, D.G., Vellinga, A., Hage, S., Acikalin, S., Bailey, L., Chapplow, N., Chen, Y., Eggenhuisen, J.T., Hendry, A., Heerema, C., J., Heijnen, Hubbard, S.M., Hunt, J.E., McGhee, C., Parsons, D.R., Simmons, S.M., M., Stacey, C.D., Vendettuoli, D. (in review, Science Advance). First source-to-sink monitoring shows dense head controls sediment flux and runout in turbidity currents.
52. Prior, D. B., Bornhold, B. D., & Johns, M. W. (1986). Active sand transport along a fjord-bottom channel, Bute Inlet, British Columbia. *Geology*, 14(7), 581-584.
53. Prior, D. B., Bornholdt, B. D., Wiseman, W. J. J., & Lowe, D. R. (1987). Turbidity Current Activity in a British Columbia Fjord. *Sciences, New Serie, American Association for the Advancement of Science, 237*(4820), 1330-1333.
54. Runkel, R.L., Crawford, C.G., and Cohn, T.A., 2004, Load Estimator (LOADEST):
    A FORTRAN Program for Estimating Constituent Loads in Streams and Rivers: U.S. *Geological Survey Techniques and Methods Book 4*, Chapter A5, 69 p.
55. Sadler, P. M. (1981). Sediment Accumulation Rates and the Completeness of Stratigraphic Sections. *The Journal of Geology, 89(5),* 569–584. doi:10.1086/628623
56. Smeaton, C., & Austin, W. E. N. (2019). Where's the Carbon: Exploring the Spatial Heterogeneity of Sedimentary Carbon in Mid-Latitude Fjords. *Frontiers in Earth Science*, 7, 269.

57. Smith, R. W., Bianchi, T. S., Allison, M., Savage, C., & Galy, V. (2015). High rates of organic carbon burial in fjord sediments globally. *Nature Geoscience, 8*. doi:10.1038/ngeo2421.
58. Soulet, G., Skinner, L., Beaupré, S.R., Galy, V. 2016. A note on reporting of reservoir ^{14}C disequilibria and age offsets. *Radiocarbon*, 58 (1), 205-2011.
59. Sparkes, R. B., Lin, I.-T., Hovius, N., Galy, A., Liu, J. T., Xu, X., & Yang, R. (2015). Redistribution of multi-phase particulate organic carbon in a marine shelf and canyon system during an exceptional river flood: Effects of Typhoon Morakot on the Gaoping River–Canyon system. *Marine Geology, 363*, 191-201. doi:10.1016/j.margeo.2015.02.013
60. Sparkes, R. B. (2012). Marine Sequestration of Particulate Organic Carbon from Mountain Belts. (PhD thesis) Downing College, University of Cambridge, United Kingdom
61. Syvitski, J. P. M., & Farrow, G. E. (1983). Structures and processes in Bayhead Deltas: Knight and Bute Inlet, British Columbia. *Sedimentary Geology, 36*(217), 244.
62. Syvitski, J. P. M., Asprey, K. W., Clattenburg, D. A., & Hodge, G. D. (1985). The prodelta environment of a fjord: suspended particle dynamics. *Sedimentology, 32*, 83-107.
63. Syvitski, J. P. M., Smith, J.N., Calabrese, E.A., Boudreau, B.P. (1988). Basin Sedimentation and the Growth of Prograding Deltas. *Jounral of Geophysical Research, 93 (C6)*, 6895-6908.
64. Tabata, S., & Pickard, G. L. (1957). The physical oceanography of Bute Inlet, British Columbia. *Journal of the Fisheries Research Board of Canada*, *14*(4), 487–520. https://doi.org/10.1139/f57-014
65. Talling, P. J., Amy, L. A., & Wynn, R. B. (2007). New insight into the evolution of large-volume turbidity currents: comparison of turbidite shape and previous modelling results. *Sedimentology*, 54(4), 737-769.
66. Talling, P. J., Massin, D., G., Sumner, E. J., & Malgesini, G. (2012). Subaqueous sediment density flows: Depositional processes and deposit types. *Sedimentology*, 59, 1937–2003. doi:10.1111/j.1365-3091.2012.01353.x
67. Turowski, J.M., Hilton, R.G., Sparker, R. (2016). Decadal carbon discharge by a mountain stream is dominated by coarse organic matter. *Geology*, 44 (1), p. 27-30.

68. Underwood, G., Paterson, D. and Parkes, R. (1995). The measurement of microbial carbohydrate exopolymers from intertidal sediments. *Limnology and Oceanography,* 40(7), pp.1243-1253.
69. Water Survey of Canada. (2020). Historical Hydrometric Data.
70. Waterson, E. J., & Canuel, E. A. (2008). Sources of sedimentary organic matter in the Mississippi River and adjacent Gulf of Mexico as revealed by lipid biomarker and $\delta^{13}C$ TOC analyses. *Organic Geochemistry*, 39(4), 422-439.
71. West, A. J., Lin, C. W., Lin, T. C., Hilton, R. G., Liu, S. H., Chang, C. T., Lin, K.-C., Galy, A., Sparkes, R.B., Hovius, N. (2011). Mobilization and transport of coarse woody debris to the oceans triggered by an extreme tropical storm. *Limnology and oceanography*, 56(1), 77-85.
72. Włodarska-Kowalczuk, M., Mazurkiewicz, M., Górska, B., Michel, L. N., Jankowska, E., & Zaborska, A. (2019). Organic carbon origin, benthic faunal consumption, and burial in sediments of northern Atlantic and Arctic fjords (60–81°N). *Journal of Geophysical Research: Biogeosciences*, 124, 3737–3751. https://doi.org/10.1029/2019JG005140
73. Zeng, J., Lowe, D. R., B., P. D., Wiseman, W. J. J., & Bornhold, B. D. (1991). Flow properties of turbidity currents in Bute Inlet, British Columbia. *Sedimentology,* 38(6), 975-996.

Journal of Geophysical Research: Biogeosciences

Supporting Information for

How turbidity currents dictate organic carbon fluxes across river-fed fjords

S. Hage[1,2,3*], V.V. Galy[4], M.J.B. Cartigny[5], C. Heerema[5], M.S. Heijnen[6], S. Acikalin[7], M.A. Clare[6], I. Giesbrecht[8], D.R. Gröcke[9], A. Hendry[7], R. G. Hilton[5,10], S.M. Hubbard[1], J.E. Hunt[6], D.G. Lintern[11], C. McGhee[7], D.R. Parsons[12], E. L. Pope[5], C D. Stacey[11], E.J. Sumner[3], S. Tank[8], P.J. Talling[5]

[1]Department of Geoscience, University of Calgary, Canada

[2]Géosciences Marines, Ifremer, France

[3]School of Ocean and Earth Sciences, University of Southampton, UK

[4]Department of Marine Chemistry and Geochemistry, Woods Hole Oceanographic Institution

[5]Department of Geography, Durham University, UK[6]National Oceanography Centre Southampton, UK

[7]School of Natural and Environmental Sciences, Newcastle University, UK

[8]Hakai Institute, Victoria, BC, Canada,

[9]Department of Earth Sciences, Durham University, UK

[10]Department of Earth Sciences, University of Oxford, UK

[11]Geological Survey of Canada, Natural Resources Canada, Sidney, British Columbia

[12]Energy and Environment Institute, University of Hull, UK

*Corresponding author: Sophie Hage (sophie.hage@ifremer.fr)

Contents of this file

Introduction

The following information contains supplementary description of the methods used to estimate the river flow and sediment discharge (Text S1 to S3), and the approaches used to determine sedimentation rates in the seabed of Bute Inlet (Text S4 and S5). Five supplementary figures, five equations and five tables are also included.

Text S1: Flow discharge of Homathko and Southgate Rivers

The Homathko River has been gauged by Water Survey of Canada for decades while the Southgate River was not gauged until late June 2021 (Fig. S1). Therefore, in order to estimate the Southgate discharge in our year of sampling (2017), we developed a linear regression model that predicted Southgate discharge from Homathko discharge using all available overlapping flow observations as of late October 2021 (Fig. S2a). The training dataset contained n = 123 daily flow observations spanning a broad range of flows from record high discharge in late June 2021 through moderately low flows in October 2021. The resulting model had a good overall fit (10 fold cross-validated RMSE = 22.2; R^2 = 0.98; Fig. S2b) and was used to backcast Southgate River discharge for 2017 (Fig. S3). In each river, the gauge was located several km upstream of the outlet and thus missed small tributaries near the mouth. Consequently, we scaled up from discharge estimates at the gauges to discharge estimates at the watershed outlets using the watershed to gauged area ratios (the Homathko watershed is 98 % gauged, whereas the Southgate watershed is 87 % gauged).

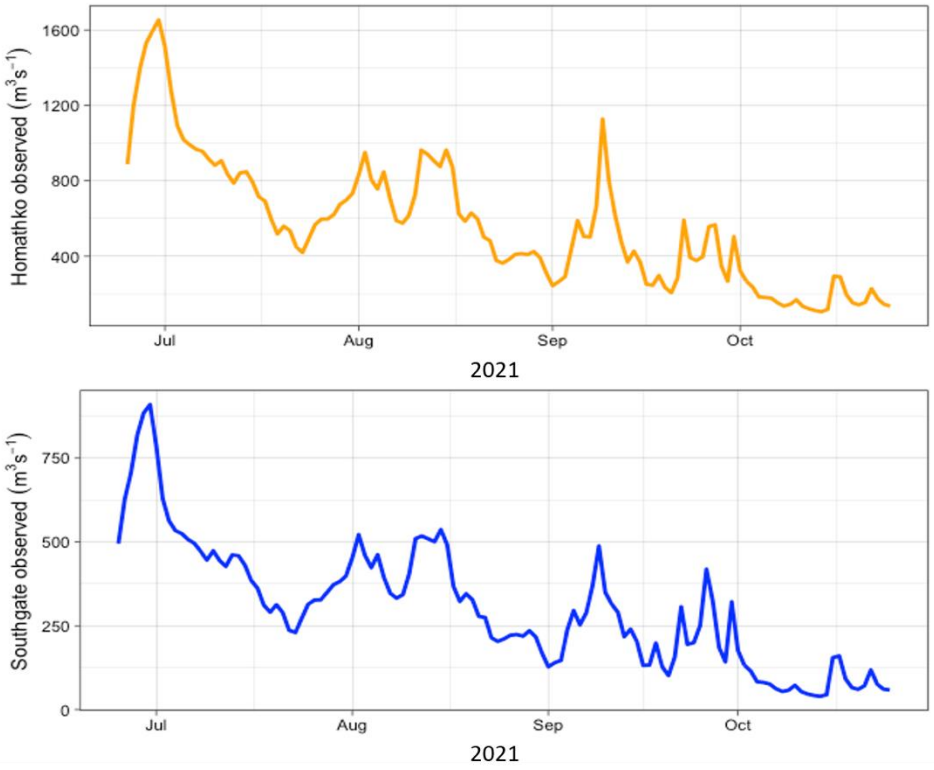

Figure S1. Flow discharge data collected between June 2021 and October 2021 by the Water Survey of Canada gauging stations on the Homathko and Southgate Rivers.

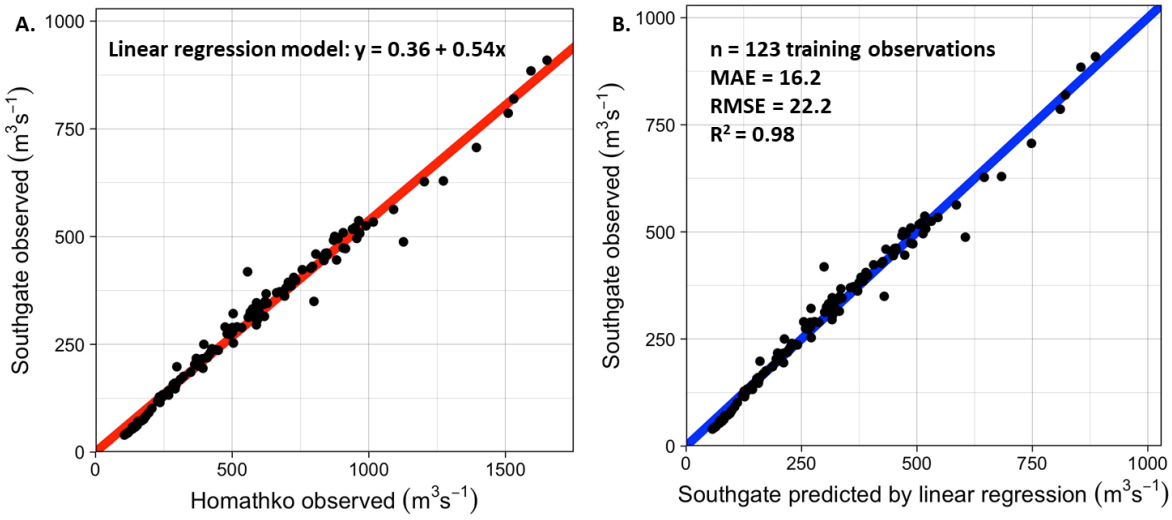

Figure S2. A. Relationship between flow discharge observations in the Homathko and Southgate River in 2021. **B.** Comparison between Southgate flow predicted by linear regression (in A) and Southgate flow observed at the gauging station (Fig. S1). The blue line is a 1:1 line representing 100% accurate prediction. MAE = mean absolute error, RMSE = root-mean-squared error, R^2 = coefficient of determination.

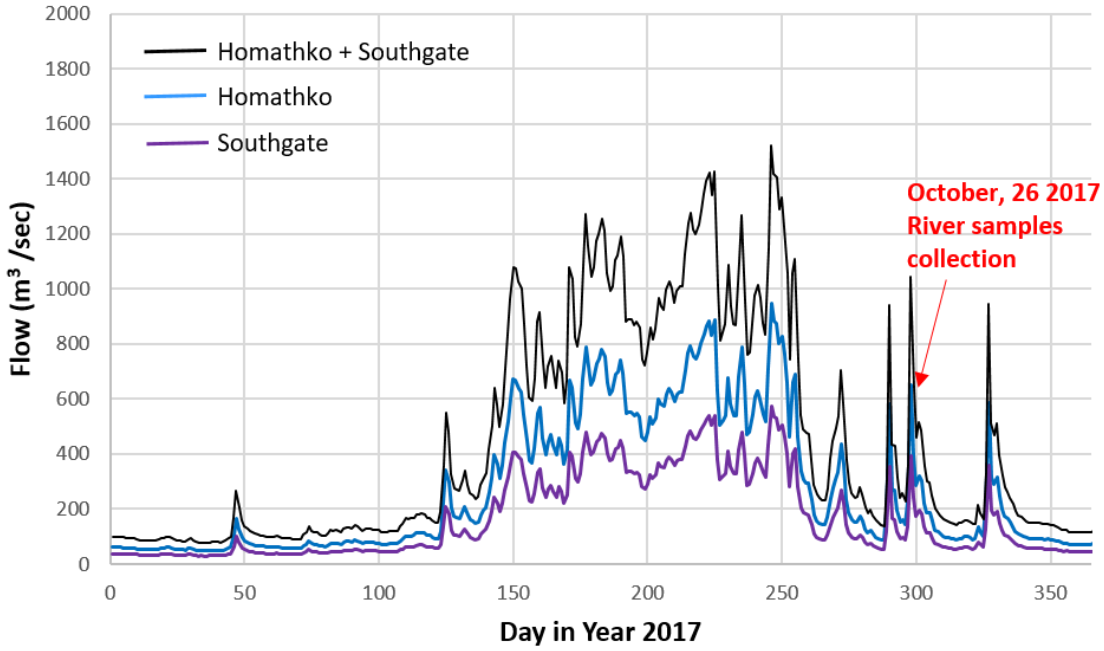

Figure S3. Flow discharge for the Homathko and Southgate Rivers observed and modelled for the year 2017.

Text S2: Bedload discharge of the Homathko and Southgate Rivers

Bedload discharge for the Homathko River was estimated at 99 kg/sec by Syvitski and Farrow (1983) which equates to 3122 x 10^6 kg/yr. No estimate was found in the literature for the Southgate river bedload discharge. We thus used the ratio between the two river watersheds (Eq. 1) as a scaling factor to deduce an annual mean river bedload for the Southgate using the Homathko bedload estimate. This gives a Southgate bedload annual discharge of 1073 x 10^6 kg/yr. In total, the bedload discharge brought in by the two rivers equals 4164 Kt/yr.

Because the Southgate bedload discharge is estimated based on the Homathko bedload discharge, we use the average total organic carbon of the samples collected in the bedload of both rivers (i.e. TOC = 0.35 ± 0.1 %, Table S7) to derive a total OC bedload flux. This gives a total organic carbon bedload flux of 14.9 ± 3.6 Kt OC /yr for the Homathko and Southgate rivers.

$$\frac{5782}{1985}\frac{km^2}{km^2} = 2.91$$

Equation S1. Ratio between the Homathko and the Southgate Rivers' watersheds

$$\frac{3122}{2.91} \text{ x } 10^6 \text{ kg/yr} = 1073 \text{ x } 10^6 \text{ kg/yr}$$

Equation S2. Southgate River annual bedload flux predicted based on the Homathko River bedload flux

Syvitski, J. P. M., & Farrow, G. E. (1983). Structures and processes in Bayhead Deltas: Knight and Bute Inlet, British Columbia. Sedimentary Geology, 36(217), 244.

Text S3: Total suspended sediment (TSS) load discharge of the Homathko and Southgate Rivers

A total of 34 and 20 suspended sediment samples were collected by the Hakai Institute between 2016 and 2021 in the Homathko and Southgate Rivers, respectively (Tables S1 and S2). Constituent concentrations and flow discharge were measured for each sample. Based on these physical samples and on the water discharge data presented in Text S1, we modeled monthly and annual constituent fluxes using the USGS LOADEST program (Runkel et al., 2004). LOADEST uses a time series of paired streamflow and constituent concentration data to construct a calibration regression, which is then applied to a daily discharge record to obtain daily constituent fluxes (load; mass day-1). The program uses a series of models which are nested within Equation S3.

$$\ln Load = a_0 + a_1 \ln Q + a_2 \ln Q^2 + a_3 \sin(2\pi dtime) + a_4 \cos(2\pi dtime) + a_5 dtime + a_6 dtime^2$$

Equation S3. Equation used by the LOADEST program to model monthly and annual TSS discharge for the Homathko and Southgate Rivers. lnLoad = the natural log of Load, lnQ = [ln(streamflow) - center of ln(streamflow)], and dtime = [decimal time - center of decimal time].

We used the AIC criteria to select the model of best fit from among the nested series of potential models, following common practice when there is no a priori reason for model preference (Burnham and Anderson, 2002).

In total, we estimate an annual mean suspended load of 30.9 kg/sec for the Homathko River, averaged between years 2016 to 2020. This number is almost equal to the previous estimate of 29 kg/sec made on the Homathko River by Syvitski and Farrow (1983). The annual mean suspended load of the Southgate River is estimated at 7 kg/sec averaged between 2017 and 2020.

Runkel, R.L., Crawford, C.G., and Cohn, T.A., 2004, Load Estimator (LOADEST): A FORTRAN Program for Estimating Constituent Loads in Streams and Rivers: U.S. Geological Survey Techniques and Methods Book 4, Chapter A5, 69 p.

Burnham, K. P., & Anderson, D. R., 2002. A practical information-theoretic approach. Model selection and multimodel inference, 2.

Syvitski, J. P. M., & Farrow, G. E. (1983). Structures and processes in Bayhead Deltas: Knight and Bute Inlet, British Columbia. Sedimentary Geology, 36(217), 244.

Site	Date	Time	Flow (ft^3/sec)	Conc. (mg/l)
Homathko	04/30/2016	1200	7275	37,4
Homathko	06/02/2018	1200	10877	46,6
Homathko	07/31/2018	1200	32454	316,0
Homathko	08/29/2018	1200	20129	70,5
Homathko	09/19/2018	1200	5544	5,2
Homathko	10/23/2018	1200	3521	7,1
Homathko	11/27/2018	1200	8581	62,5
Homathko	01/28/2019	1200	1978	4,4
Homathko	05/16/2019	1200	9712	41,4
Homathko	06/25/2019	1200	12784	36,8
Homathko	07/16/2019	1200	18717	58,3
Homathko	08/22/2019	1200	19882	219,7
Homathko	09/19/2019	1200	9217	78,8
Homathko	10/10/2019	1200	4202	32,2
Homathko	10/18/2019	1200	6427	38,8
Homathko	11/07/2019	1200	3267	13,5
Homathko	12/05/2019	1200	2423	8,0
Homathko	01/21/2020	1200	2373	31,9
Homathko	02/18/2020	1200	1801	3,0
Homathko	03/16/2020	1200	1434	2,6
Homathko	06/03/2020	1200	12643	55,7
Homathko	07/09/2020	1200	17340	66,6
Homathko	08/12/2020	1200	12572	91,6
Homathko	10/22/2020	1200	5756	33,8
Homathko	12/17/2020	1200	3955	9,0
Homathko	01/13/2021	1200	3343	14,9
Homathko	02/09/2021	1200	1711	4,0
Homathko	03/10/2021	1200	1518	3,3
Homathko	04/20/2021	1200	5240	21,2
Homathko	05/20/2021	1200	7500	29,0
Homathko	06/15/2021	1200	14630	73,1
Homathko	07/13/2021	1200	29709	162,1
Homathko	08/11/2021	1200	34016	238,6
Homathko	10/07/2021	1200	5372	17,6

Table S1. Suspended sediment samples collected in the Homathko River between 2016 and 2021. Flow discharge are given in cubic feet per second and concentrations (Conc.) in milligram per liter)

Site	Date	Time	Flow (ft^3/sec)	Conc. (mg/l)
Southgate	04/30/2018	1200	3915	16,5
Southgate	06/02/2018	1200	5847	29,9
Southgate	08/29/2018	1200	10810	37,9
Southgate	09/19/2018	1200	2987	3,5
Southgate	10/23/2018	1200	1901	6,1
Southgate	03/28/2019	1200	1280	2,9
Southgate	06/25/2019	1200	6870	25,1
Southgate	12/17/2020	1200	2134	5,7
Southgate	01/13/2021	1200	1806	4,4
Southgate	02/09/2021	1200	931	3,1
Southgate	03/10/2021	1200	827	2,3
Southgate	04/20/2021	1200	2824	13,3
Southgate	05/20/2021	1200	4035	47,7
Southgate	06/15/2021	1200	7860	88,2
Southgate	06/30/2021	1200	32107	526,4
Southgate	07/13/2021	1200	16288	61,3
Southgate	08/10/2021	1200	14314	131,7
Southgate	08/11/2021	1200	18010	237,9
Southgate	09/30/2021	1200	11347	49,9
Southgate	10/07/2021	1200	2192	35,7

Table S2. Suspended sediment samples collected in the Southgate River between 2018 and 2021. Flow discharge are given in cubic feet per second and concentrations (Conc.) in milligram per liter)

Text S4: Sedimentation rate based on bathymetric difference maps

The first approach to determine sedimentation rates in Bute Inlet uses differences between two bathymetric surveys obtained in 2008 and 2018, and analyzed by Heijnen et al. (in review). This approach derived sediment volumes in the channel and lobe of Bute Inlet, showing that sediment is transported stepwise down the channel as a result of turbidity currents becoming less frequent along the channel transect. Previous work in the same channel highlighted zones of erosion and deposition that migrate upstream significantly (100 to 450 m per year) due to the presence of turbidity current-related knickpoints (Heijnen et al., 2020). Overall, the channel has a net eroded volume of 41 ± 12 Mm^3 and a net deposited volume of 19 ± 12 Mm^3 between 2008 and 2018 (Table S3; Heijnen et al., in review). The lobe shows no erosion and a total deposition of 30 ± 38 Mm^3 between 2008 and 2018 (Table S3; Heijnen et al., in review). Volume uncertainties are based on vertical accuracy of the multibeam surveys of 0.5 % of the water depth, hence the 600 m deep lobe is greatly affected (Heijnen et al., 2020). We divided these net 2008-2018 sediment volumes by the surface areas of the channel and lobe, to derive annual sedimentation rates of -16 ± 9 cm/yr and 18 ± 9 cm/yr, respectively (Table S4).

Comparison between the sources of sediment available in the Bute submarine system (i.e. supplied by the rivers and made available through erosion in the channel; Table S4) and sediment deposited on the seabed on the channel and lobe results in a sediment deficit of 3.1 ± 0.9 Mm^3/yr (Table S4). If we assume that this deficit is spread over the overbanks and distal flat basin (i.e. outside of channe and lobe; Heijnen et al., in review), and that we divide this deficit by the surface area of the overbanks and distal flat basin, we find a sedimentation rate of 2 ± 0.6 cm/yr in these two sub-environments (Table S4).

Heijnen, M. S., Clare, M.A., Cartigny, M. J., Talling, P.J., Hage, S., Pope, E.L., Bailey, L., Sumner, E.J., Lintern, D.G., Stacey, C.D., Parsons, D.P., Simmons, S.M., Chen, Y., Hubbard, S.M., Eggenhuisen, J.T., Kane, I., Hughes Clarke, J.E. (in review, EPSL) Fill, flush or shuffle: How is sediment carried through submarine channels to build lobes?

Heijnen, M. S., Clare, M. A., Cartigny, M. J., Talling, P. J., Hage, S., Lintern, D. G., Stacey, C.D., Parsons, D.R., Simmons, S.M., Chen, Y., Sumner, E.J., Dix, J.K., Hughes Clarke, J.E. (2020). Rapidly-migrating and internally-generated knickpoints can control submarine channel evolution. Nature communications, 11(1), 1-15.

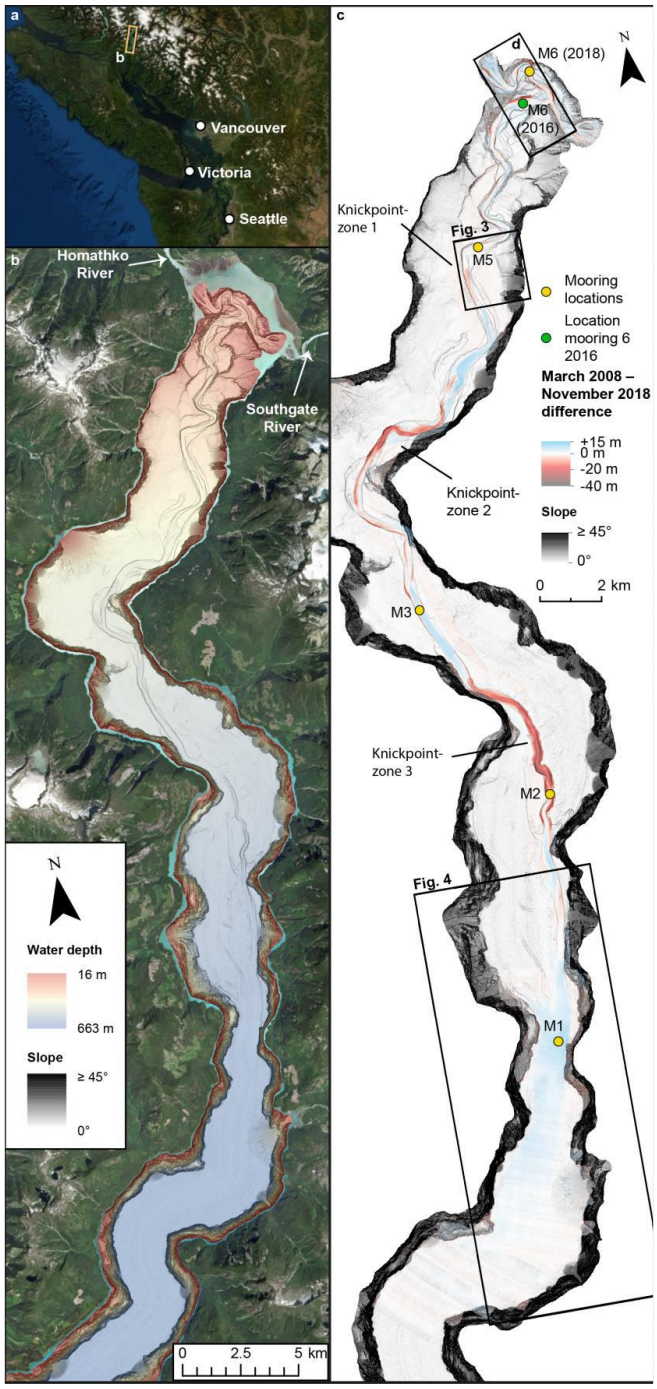

Figure S4. Location, bathymetry and 2008 to 2018 difference maps modified from Heijnen et al. (in review). **A.** Location of Bute Inlet. **B.** Overview of the submarine channel-lobe system in Bute Inlet as monitored in March 2008. Data is presented as a slope map overlain by a semi-transparent bathymetry map. **C.** 2008 slope map overlain by a March 2008 – November 2018

difference map. Note the along channel alternation of erosional and depositional areas controlled by knickpoints.

Heijnen et al. (in review)		
Sub-environment	**Volume of sediment sources 2008-2018** (eroded from seabed)	**Volume of sediment deposited on the seabed between 2008 and 2018**
Channel	41 ± 12 Mm^3	19 ± 11 Mm^3
Lobe	No net erosion	30 ± 38 Mm^3
Total	41 ± 12 Mm^3	49 Mm^3

Table S3. Sediment budgets in the channel and lobe between March 2008 and November 2018 (modified from Heijnen et al., in review).

Sub-environment	Annual net sediment volume budget (Mm^3/yr)	Surface area (km^2)	Annual sedimentation rate (cm/yr)
Homathko and Southgate Rivers	3.8 ± 2.5	n/a	n/a
Channel	-2.0 ± 1 (-3.7 + 1.7)	12.2	**-16 ± 9**
Lobe	2.7 ± 3.4	15.4	**18 ± 22**
Total sediment sources (i.e. eroded from seabed and supplied by rivers)	7.5 ± 3.6	n/a	n/a
Total deposited sediment	4.5 ± 4.5	n/a	n/a
Deficit between sources and deposits	3.1 ± 0.9	n/a	n/a
Deficit spread over overbanks and distal flat basin	3.1 ± 0.9	133	**2.3 ± 0.6**

Table S4. Annual sediment budgets and annual sedimentation rates in the Bue Inlet sub-environments, obtained based on time-lapse bathymetry presented in Heijnen et al. (in review; Table S3). Sediment volume delivered by the rivers is represented as the river sediment load volume if it were deposited using a sediment density of 2585 kg/m^3 and a porosity of 30 to 60 %.

Text S5: Sedimentation rates based on ^{210}Pb dating

A second approach, holding for a centennial timescale, was used to determine sedimentation rates in the Bute Inlet sub-environments, based on previous work (Syvistki et al., 1988; Heerema, 2021). ^{210}Pb dating was performed in Bute Inlet on five sediment cores collected in the overbanks and on one sediment core collected in the distal flat basin (Fig. S5). A sedimentation model was also developed on two sediment cores in the overbanks by Syvitski et al. (1987), allowing comparison between two methods on these cores (Fig. S5, Table S4). We computed the average between the sedimentation rates presented in Syvistki et al. (1988) and Heerema (2021), to derive a mean sedimentation rate of 2 ± 1.5 cm/yr in the overbanks and 1 ± 0.3 cm/yr in the distal flat basin (Table S4). These sedimentation rates are lower compared to the sedimentation rates derived for the overbanks and distal flat basin by time-lapse bathymetry (i.e. Approach 1; Text S4). This trend of falling mean sedimentation rate with increasing time span was previously highlighted globally, under the so-called "Sadler effect" (Sadler, 1981).

Mean sedimentation rate in the depositional lobe is also expected to decrease with increasing time span for which the lobe is considered (Sadler, 1981). No dating was performed on the cores collected in the lobe, nor the channel, as these environments are too sandy. Instead, we used an assumed relationship between the sedimentation rate obtained in the overbank and that of the channel and lobe (Equations S4 and S5).

$$\mathbf{C_{SR}} = 0.35 * O_{SR} = 0.35 * 2 \pm 1.5 = \mathbf{0.7} \pm 0.5 \ \mathbf{cm/yr}$$

Equation S4. Assumed relationship between sedimentation rate in the channel (C_{SR}) and in the overbank (O_{SR})

$$\mathbf{L_{SR}} = 5 * O_{SR} = 5 * 2 \pm 1.5 = \mathbf{10} \pm 7.5 \ \mathbf{cm/yr}$$

Equation S5. Assumed relationship between sedimentation rate in the lobe (L_{SR}) and in the overbank (O_{SR})

These relationships are based on the relationships between overbanks and channel/lobe found in the Congo turbidity current system (Baudin et al., 2020). We acknowledge that the Congo system is different (e.g. scale, composition) compared to the Bute system. However, Baudin et al. (2020) is the only study, to our knowledge, that provides separate sedimentation rates for the different turbidity current sub-environments over centennial timescales. Furthermore, it seems reasonable to assume that the Bute channel will likely reach a net positive sedimentation rate

close to zero over centennial timescales. Indeed, if the channel were to keep a negative sedimentation rate (as suggested by the time-lapse bathymetry in Text S4), we would expect to see a canyon rather than a channel in the Bute turbidity current system (Deptuck et al., 2003). The 10 cm/yr sedimentation rate found in the lobe for a centennial timescale is lower compared to the 18 cm/yr found for a decennial timescale (Text S4), which is line with the Sadler effect (Sadler, 1981).

Baudin, F., Rabouille, C., & Dennielou, B. (2020). Routing of terrestrial organic matter from the Congo River to the ultimate sink in the abyss: a mass balance approach (André Dumont medallist lecture 2017). Geologica Belgica, 23(1-2).

Deptuck, M.E., Steffens, G.S., Barton, M., Pirmez, C. (2003) Architecture and evolution of upper fan channel-belts on the Niger Delta slope and in the Arabian Sea. Marine and Petroleum Geology 20, 649-676.

Heerema, C. J. (2021). Evolution of Turbidity Currents: New insights from direct field measurements, Durham theses, Durham University. Available at Durham E-Theses Online: http://etheses.dur.ac.uk/13963/

Sadler, P. M. (1981). Sediment Accumulation Rates and the Completeness of Stratigraphic Sections. The Journal of Geology, 89(5), 569–584. doi:10.1086/628623

Syvitski, J. P. M., Smith, J.N., Calabrese, E.A., Boudreau, B.P. (1988). Basin Sedimentation and the Growth of Prograding Deltas. Journal of Geophysical Research, 93 (C6), 6895-6908.

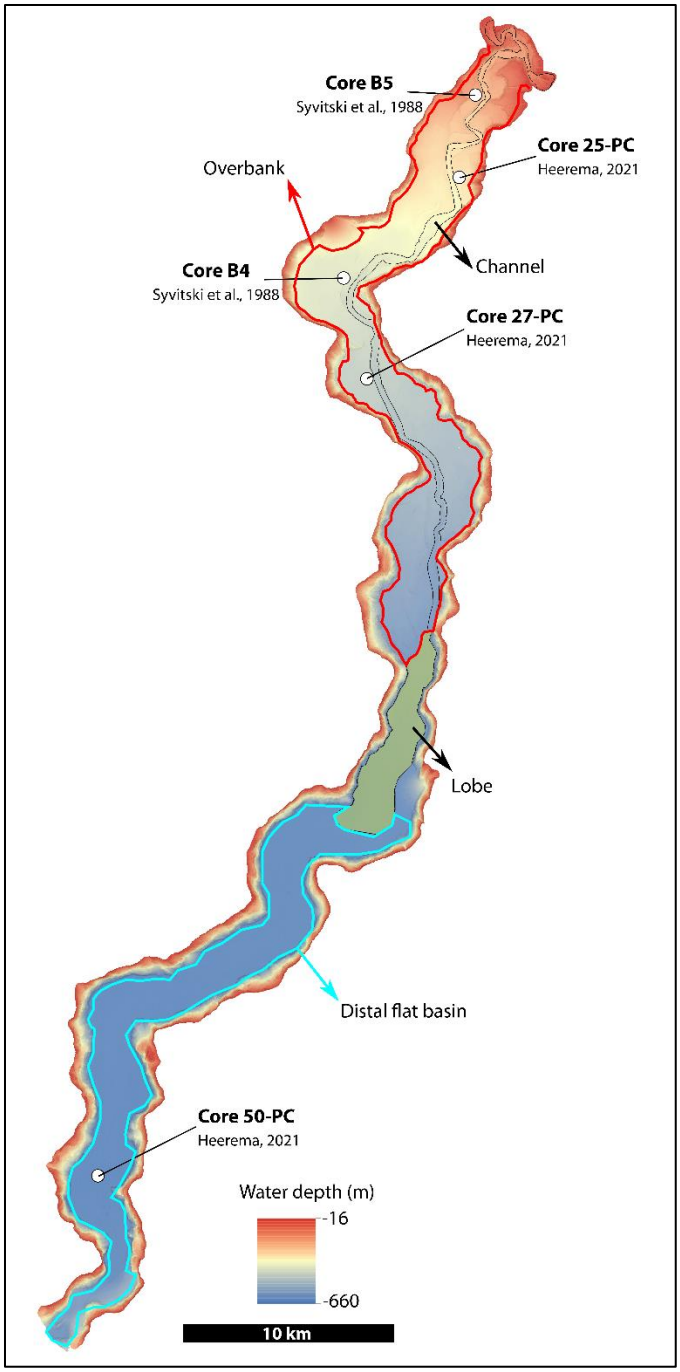

Figure S5. Location of the sediment cores previously dated by Syvitski et al. (1988) and Heerema (2021).

Core and reference	^{210}Pb sedimentation rate (cm/yr)	Model sedimentation rate (cm/yr)	Sub-environment (Location Fig. S5)	Average (cm/yr)
B5 Syvistki et al., 1988	4.56	3.78	Overbanks	**2 ± 1.5** (n=7)
25-PC Heerema, 2021	1.2 (γ) 0.9 (α)	-	Overbanks	
B4 Syvistki et al., 1988	1.14	1.11	Overbanks	
27-PC Heerema, 2021	0.9 (γ)	-	Overbanks	
50-PC Heerema, 2021	0.9 (γ) 1 (α)	-	Distal flat basin	**1 ± 0.5** (n=2)

Table S5. ^{210}Pb-determined and modelled sedimentation rates on five sediment cores displayed in Fig. S5 (Syvistki et al., 1988, Heerema, 2021). Gamma (γ) and alpha (α) spectrometry sedimentation are given where calculated

Text S6: Mixing model to determine the terrestrial versus marine organic carbon contribution in the samples collected from the fjord distal flat basin

We have used a simple binary (i.e. 2 end-members) mixing model to discriminate between terrestrial and marine organic carbon in the samples collected from the fjord distal flat basin. The carbon stable isotopes compositions ($\delta^{13}C$) of each sample and of two fixed end-members were used to run the model, following equations S6 and S7 (Hilton et al., 2015).

$$F_{terr} = \frac{\delta^{13}C_{sample} - \delta^{13}C_{mar}}{\delta^{13}C_{terr} - \delta^{13}C_{mar}} \times 100$$

Equation S6. Equation used to derive the fraction of terrestrial organic carbon contained in a sample.

$$F_{terr} + F_{mar} = 100$$

Equation S7. The contribution of marine and terrestrial organic carbon represents 100 % of the total organic carbon held in a sample.

Where:

- F_{terr} is the fraction of terrestrial organic carbon in %,
- F_{mar} is the fraction of marine organic carbon in %,
- $\delta^{13}C_{sample}$ is the measured carbon stable isotope composition of a sample in ‰,
- $\delta^{13}C_{mar}$ is the carbon stable isotope composition of the marine end-member, fixed at -20.5 ‰ (i.e., the minimum value measured on samples collected in the distal basin core)
- $\delta^{13}C_{terr}$ is the carbon stable isotope composition of the terrestrial end-member, fixed at -27 ‰ (Hecky and Hesslein, 1995)

Applying these equations to the samples collected in the distal flat basin results in a mean relative terrestrial contribution of 46 % (Table S6). Therefore, we estimate that about 44 % of the organic carbon found in the upper two meter sediment of the distal flat basin is of marine origin.

Hecky, R.E. and Hesslein, R.H. Contributions of Benthic Algae to Lake Food Webs as Revealed by Stable Isotope Analysis (1995). *J. N. Am. Benthol. Soc.,* 14(4):631-653

Hilton, R., Galy, V., Gaillardet, J. et al. Erosion of organic carbon in the Arctic as a geological carbon dioxide sink. Nature 524, 84–87 (2015). https://doi.org/10.1038/nature14653

Macdonald, R., Macdonald, D., O'Brien, M., & Gobeil, C. (1991). Accumulation of heavy metals (Pb, Zn, Cu, Cd), carbon and nitrogen in sediments from Strait of Georgia, BC, Canada. Marine Chemistry, 34(1-2), 109-135.

Sample depth (cm)	$\delta^{13}C_{sample}$ (‰)	F_{terr} (%)	F_{mar} (%)
20	-23,01	39	61
21	-23,37	44	56
30	-25,69	80	20
33	-25,83	82	18
37	-22,18	26	74
57	-25,25	73	27
63	-24,11	56	44
73	-21,79	20	80
86	-23,99	54	46
90	-26,03	85	15
104	-23,93	53	47
121	-23,72	50	50
151	-23,29	43	57
177	-22,40	29	71
183	-20,51	0	100
196	-22,55	32	68
197	-22,53	31	69
200	-22,17	26	74
	Mean	**46**	**54**

Table S6. Mixing model applied on sediment samples collected in the distal flat basin of Bute Inlet (i.e. core 15 in Fig. 3) following Equations S6 and S7. $\delta^{13}C$ = carbon stable isotope composition measured on each sample. F_{terr} = fraction of terrestrial organic carbon in each sample. F_{mar} = fraction of marine organic carbon in each sample.

Cruise number	Sample code	River	Environment	TOC (%)	$\delta^{13}C$ (‰)[a]	R (^{14}C yr)[b]	D_{50} (µm)	D_{90} (µm)	Latitude (°)	Longitude (°)
PGC-2017-005	RW18a	Homathko	water column	0.70	-25.05	29	45	155	50.948	-124.861
PGC-2017-005	RW20	Homathko	water column	0.64	-23.85		37	247	50.934	-124.863
PGC-2017-005	RB16	Homathko	river bank	0.09	-27.04		104	207	50.941	-124.857
PGC-2017-005	RB18	Homathko	river bank	0.17	-26.78		78	185	50.948	-124.861
PGC-2017-005	RB22	Homathko	river bank	0.25	-27.19		65	174	50.941	-124.857
PGC-2017-005	RD6	Homathko	delta	0.18	-26.71		75	230	50.9	-124.9
PGC-2017-005	RD8	Homathko	delta	0.04	-27.21		347	770	50.919	-124.848
PGC-2017-005	RP7a	Homathko	plume	1.77	-17.15		26	140	50.919	-124.848
PGC-2017-005	RP9a	Homathko	plume	2.90	-16.27				50.919	-124.848
PGC-2017-005	RP11a	Homathko	plume	2.86	-13.07				50.920	-124.844
PGC-2017-005	RW16a	Homathko	plume	1.56	-16.82				50.941	-124.857
PGC-2017-005	RW17a	Homathko	plume	1.82	-18.60				50.944	-124.858
PGC-2017-005	RW23a	Southgate	water column	1.42	-25.24				50.886	-124.797
PGC-2017-005	RW23b	Southgate	water column	0.85	-25.83	795	13	56	50.886	-124.797
PGC-2017-005	RW23c	Southgate	water column	0.91	-25.56				50.886	-124.797
PGC-2017-005	RW23d	Southgate	water column	0.70	-25.91		39	209	50.886	-124.797
PGC-2017-005	RB24	Southgate	river bank	0.69	-27.45		173	331	50.888	-124.797
PGC-2017-005	RD12	Southgate	delta	0.41	-26.23		37	159	50.891	-124.804
PGC-2017-005	RD14	Southgate	delta	0.57	-26.74		183	493	50.895	-124.800
PGC-2017-005	RP13a	Southgate	plume	3.14	-19.44				50.891	-124.804
PGC-2017-005	RP15a	Southgate	plume	4.99	-17.95				50.895	-124.800
PGC-2017-005	RW19a	Southgate	plume	1.27	-19.82		33	214	50.938	-124.855

Table S7. Organic geochemistry, grain size, location and metadata associated with the river samples presented in this study. a: carbon stable isotopes $\delta^{13}C$ values are reported relative to Vienna Pee-Dee Belemnite (VDBP). b: R stands for reservoir age offset, reported in ^{14}C years and calculated following Soulet et al. (2016).

Core number in paper	Cruise number	Station number	Core type	Depth in core (cm)	Sub-Environment	TOC (%)	$\delta^{13}C$ (‰)[a]	R (^{14}C yr)[b]	D_{50} (µm)	D_{90} (µm)	Latitude (°)	Longitude (°)	Water depth (m)
1	PGC-2016-007	STN028	Box	3 to 7	Channel	0.03	-27.3				50.904	-124.834	227
1	PGC-2016-007	STN028	Box	20 to 24	Channel	0.19	-27.7				50.904	-124.834	227
1	PGC-2016-007	STN028	Box	4	Channel	0.26	-26.9		84	169	50.904	-124.834	227
1	PGC-2016-007	STN028	Box	9	Channel	0.03	-25.7		262	1214	50.904	-124.834	227
1	PGC-2016-007	STN028	Box	12	Channel	0.08	-26.3		624	1348	50.904	-124.834	227
1	PGC-2016-007	STN028	Box	18	Channel	0.04	-25.5		466	1333	50.904	-124.834	227
1	PGC-2016-007	STN028	Box	32	Channel	0.02	-26.3		413	1329	50.904	-124.834	227
2	PGC-2016-007	STN015	Box	2 to 6	Channel	0.27	-27.2				50.864	-124.864	319
2	PGC-2016-007	STN015	Box	18 to 22	Channel	0.03	-24.7				50.864	-124.864	319
3	PGC-2016-007	STN010	Box	0 to 4	Channel	0.37	-27.6				50.865	-124.868	322
3	PGC-2016-007	STN010	Box	15 to 19	Channel	2.70	-27.0				50.865	-124.868	322
3	PGC-2016-007	STN010	Box	24 to 28	Channel	0.03	-25.5				50.865	-124.868	322
3	PGC-2016-007	STN010	Box	2	Channel	0.35	-27.8		41	124	50.865	-124.868	322
3	PGC-2016-007	STN010	Box	6	Channel	0.55	-27.5		77	189	50.865	-124.868	322
3	PGC-2016-007	STN010	Box	20	Channel	0.03	-26.1				50.865	-124.868	322
3	PGC-2016-007	STN010	Box	26	Channel	0.02	-26.1				50.865	-124.868	322
4	PGC-2016-007	STN014	Box	0 to 4	Channel	0.03	-26.1				50.862	-124.870	322
4	PGC-2016-007	STN014	Box	17 to 21	Channel	0.03	-26.3				50.862	-124.870	322
5	PGC-2016-007	STN019	Box	1	Channel	0.56	-27.5	997	12	52	50.763	-124.915	477
5	PGC-2016-007	STN019	Box	4	Channel	0.68	-27.7	71	59	171	50.763	-124.915	477
5	PGC-2016-007	STN019	Box	10	Channel	0.92	-27.8	71			50.763	-124.915	477
5	PGC-2016-007	STN019	Box	13	Channel	0.02	-26.7		81	157	50.763	-124.915	477
5	PGC-2016-007	STN019	Box	20	Channel	0.06	-26.0	2680	172	332	50.763	-124.915	477
5	PGC-2016-007	STN019	Box	28	Channel	0.02	-25.4	3600	265	1248	50.763	-124.915	477
6	PGC-2016-007	STN014	Box	0 to 4	Channel	0.03	-26.1				50.862	-124.870	322
6	PGC-2016-007	STN014	Box	17 to 21	Channel	0.03	-26.3				50.862	-124.870	322
6	PGC-2016-007	STN025	Box	1	Channel	1.53	-28.4				50.704	-124.868	570
6	PGC-2016-007	STN025	Box	5	Channel	0.03	-26.5		70	145	50.704	-124.868	570
6	PGC-2016-007	STN025	Box	10	Channel	0.03	-26.3		78	142	50.704	-124.868	570
6	PGC-2016-007	STN025	Box	15	Channel	0.02	-26.2		109	209	50.704	-124.868	570
6	PGC-2016-007	STN025	Box	18	Channel	0.02	-26.0		193	350	50.704	-124.868	570
6	PGC-2016-007	STN025	Box	22	Channel	0.02	-26.7		316	1289	50.704	-124.868	570
7	PGC-2016-007	STN036	Box	1	Lobe	0.76	-26.8		23	104	50.633	-124.881	611
7	PGC-2016-007	STN036	Box	3	Lobe	0.42	-26.7		17	83	50.633	-124.881	611
7	PGC-2016-007	STN036	Box	4	Lobe	1.53	-27.9		61	179	50.633	-124.881	611
7	PGC-2016-007	STN036	Box	5	Lobe	0.33	-27.4				50.633	-124.881	611
7	PGC-2016-007	STN036	Box	6	Lobe	0.05	-25.5		82	160	50.633	-124.881	611
7	PGC-2016-007	STN036	Box	10	Lobe	0.03	-25.2		145	298	50.633	-124.881	611
7	PGC-2016-007	STN036	Box	15	Lobe	0.08	-27.7		137	296	50.633	-124.881	611
7	PGC-2016-007	STN036	Box	20	Lobe	0.08	-27.0		116	279	50.633	-124.881	611
7	PGC-2016-007	STN036	Box	24	Lobe	0.03	-26.5		164	1151	50.633	-124.881	611
8	PGC-2016-007	STN032	Box	10 to 14	Overbank	0.15	-26.8				50.903	-124.834	218
8	PGC-2016-007	STN032	Box	20 to 24	Overbank	0.30	-27.0				50.903	-124.834	218
8	PGC-2016-007	STN032	Box	15	Overbank	0.18	-27.5				50.903	-124.834	218
8	PGC-2016-007	STN032	Box	20	Overbank	0.17	-26.7				50.903	-124.834	218
8	PGC-2016-007	STN032	Box	22	Overbank	0.31	-26.8				50.903	-124.834	218
9	PGC-2016-007	STN031	Box	6 to 10	Overbank	0.27	-26.7				50.902	-124.835	189
9	PGC-2016-007	STN031	Box	16 to 20	Overbank	0.26	-26.7				50.902	-124.835	189
9	PGC-2016-007	STN031	Box	12	Overbank	0.26	-26.3		11	45	50.902	-124.835	189
9	PGC-2016-007	STN031	Box	24	Overbank	0.34	-27.4		13	59	50.902	-124.835	189

Table S8. Organic geochemistry, grain size, location and metadata associated with the samples collected in Bute Inlet presented in this study. a: carbon stable isotopes $\delta^{13}C$ values are reported relative to Vienna Pee-Dee Belemnite (VDBP). b: R stands for reservoir age offset, reported in ^{14}C years and calculated following Soulet et al. (2016).

Core number in paper	Cruise number	Station number	Core type	Depth in core (cm)	Sub-Environment	TOC (%)	$\delta^{13}C$ (‰)[a]	R (^{14}C yr)[b]	D_{50} (µm)	D_{90} (µm)	Latitude (°)	Longitude (°)	Water depth (m)
10	PGC-2016-007	STN029	Box	25	Overbank	0.38	-27.1				50.905	-124.833	223
10	PGC-2016-007	STN030	Box	5 to 9	Overbank	0.16	-27.3				50.903	-124.839	218
10	PGC-2016-007	STN030	Box	14 to 18	Overbank	0.27	-27.3				50.903	-124.839	218
10	PGC-2016-007	STN030	Box	7	Overbank	0.46	-27.2				50.903	-124.839	218
10	PGC-2016-007	STN030	Box	11	Overbank	0.11	-26.7				50.903	-124.839	218
10	PGC-2016-007	STN030	Box	25	Overbank	0.23	-27.0				50.903	-124.839	218
10	PGC-2016-007	STN030	Box	30	Overbank	0.21	-27.0				50.903	-124.839	218
11	PGC-2016-007	STN09	Box	0 to 4	Overbank	0.20	-27.6				50.864	-124.867	321
11	PGC-2016-007	STN09	Box	20 to 24	Overbank	0.02	-26.0				50.864	-124.867	321
11	PGC-2016-007	STN09	Box	5	Overbank	0.40	-27.9				50.864	-124.867	321
11	PGC-2016-007	STN09	Box	13	Overbank	0.10	-29.1				50.864	-124.867	321
11	PGC-2016-007	STN09	Box	15	Overbank	0.35	-27.7				50.864	-124.867	321
11	PGC-2016-007	STN09	Box	20	Overbank	0.27	-27.2				50.864	-124.867	321
11	PGC-2016-007	STN09	Box	24	Overbank	0.02	-26.0				50.864	-124.867	321
11	PGC-2016-007	STN09	Box	30	Overbank	0.38	-28.2				50.864	-124.867	321
12	PGC-2016-007	STN020	Box	2	Overbank	0.31	-26.2		69	155	50.763	-124.911	466
12	PGC-2016-007	STN020	Box	7	Overbank	0.04	-26.2				50.763	-124.911	466
12	PGC-2016-007	STN020	Box	12	Overbank	0.17	-26.0		46	134	50.763	-124.911	466
12	PGC-2016-007	STN020	Box	23	Overbank	0.03	-25.8		116	225	50.763	-124.911	466
12	PGC-2016-007	STN020	Box	32	Overbank	0.42	-26.8		22	89	50.763	-124.911	466
13	PGC-2016-007	STN021	Box	10 to 14	Overbank	0.02	-25.7				50.762	-124.918	462
13	PGC-2016-007	STN021	Box	20 to 24	Overbank	0.24	-26.6				50.762	-124.918	462
13	PGC-2016-007	STN021	Box	16	Overbank	0.25	-26.9				50.762	-124.918	462
13	PGC-2016-007	STN021	Box	9	Overbank	0.03	-24.8				50.762	-124.918	462
14	PGC-2016-007	STN026	Box	10 to 14	Overbank	0.17	-26.1				50.705	-124.865	538
14	PGC-2016-007	STN026	Box	24 to 28	Overbank	0.30	-25.9				50.705	-124.865	538
14	PGC-2016-007	STN026	Box	8	Overbank	0.33	-26.9		35	105	50.705	-124.865	538
14	PGC-2016-007	STN026	Box	14	Overbank	0.84	-28.2		125	256	50.705	-124.865	538
14	PGC-2016-007	STN026	Box	20	Overbank	0.40	-26.3				50.705	-124.865	538
14	PGC-2016-007	STN026	Box	26	Overbank	0.20	-26.7				50.705	-124.865	538
14	PGC-2016-007	STN026	Box	30	Overbank	0.10	-26.1				50.705	-124.865	538
15	PGC-2016-003	STN01	Piston	20	Distal basin	3.07	-23.01				50.420	-125.085	647
15	PGC-2016-003	STN01	Piston	21	Distal basin	2.93	-23.37				50.420	-125.085	647
15	PGC-2016-003	STN01	Piston	30	Distal basin	0.52	-25.69				50.420	-125.085	647
15	PGC-2016-003	STN01	Piston	33	Distal basin	0.52	-25.83				50.420	-125.085	647
15	PGC-2016-003	STN01	Piston	37	Distal basin	3.52	-22.18				50.420	-125.085	647
15	PGC-2016-003	STN01	Piston	57	Distal basin	0.50	-25.25				50.420	-125.085	647
15	PGC-2016-003	STN01	Piston	63	Distal basin	2.40	-24.11	523			50.420	-125.085	647
15	PGC-2016-003	STN01	Piston	73	Distal basin	2.21	-21.79				50.420	-125.085	647
15	PGC-2016-003	STN01	Piston	86	Distal basin	0.68	-23.99				50.420	-125.085	647
15	PGC-2016-003	STN01	Piston	90	Distal basin	0.46	-26.03				50.420	-125.085	647
15	PGC-2016-003	STN01	Piston	104	Distal basin	0.43	-23.93				50.420	-125.085	647
15	PGC-2016-003	STN01	Piston	121	Distal basin	0.50	-23.72				50.420	-125.085	647
15	PGC-2016-003	STN01	Piston	151	Distal basin	0.65	-23.29				50.420	-125.085	647
15	PGC-2016-003	STN01	Piston	177	Distal basin	0.57	-22.40	1080			50.420	-125.085	647
15	PGC-2016-003	STN01	Piston	183	Distal basin	2.18	-20.51	1103			50.420	-125.085	647
15	PGC-2016-003	STN01	Piston	196	Distal basin	0.61	-22.55				50.420	-125.085	647
15	PGC-2016-003	STN01	Piston	197	Distal basin	0.72	-22.53				50.420	-125.085	647
15	PGC-2016-003	STN01	Piston	200	Distal basin	0.90	-22.17				50.420	-125.085	647

Table S8 (continued). Organic geochemistry, grain size, location and metadata associated with the samples collected in Bute Inlet presented in this study. **a:** carbon stable isotopes $\delta^{13}C$ values are reported relative to Vienna Pee-Dee Belemnite (VDBP). b: R stands for reservoir age offset, reported in ^{14}C years and calculated following Soulet et al. (2016).